



Redox fluctuations, trace metal enrichment and phosphogenesis in the ~2.0 Ga Zaonega Formation



Michael A. Kipp^{a,b,1,*}, Aivo Lepland^{c,d,e,f}, Roger Buick^{a,b}

^a Department of Earth & Space Sciences, University of Washington, Seattle, WA 98195-1310, USA

^b Virtual Planetary Laboratory, NASA Nexus for Exoplanet System Science, Seattle, WA 98195-1310, USA

^c Geological Survey of Norway, 7491 Trondheim, Norway

^d Centre for Arctic Gas Hydrate, Environment and Climate, Department of Geosciences, UiT The Arctic University of Norway, 9037 Tromsø, Norway

^e University of Tartu, Department of Geology, 50411 Tartu, Estonia

^f Tallinn University of Technology, Institute of Geology, 19086 Tallinn, Estonia

A B S T R A C T

The ~2.0 Ga Zaonega Formation (ZF) holds one of the oldest phosphorites in the geologic record, reaching > 15% P₂O₅. Understanding the depositional conditions that enabled sedimentary phosphorus enrichment in this unit will thus help us to interpret the significance of the temporal distribution of phosphorites in Earth's early history. Here we use an array of major and trace element data to constrain the redox conditions in the water column and extent of basinal restriction during deposition of the ZF. We also present new selenium (Se) abundance and isotopic data to provide firmer constraints on fluctuations across high redox potentials, which might be critical for phosphogenesis. We find that Se isotope ratios shift over a range of ~3‰ in the ZF, with the earliest stratigraphically-resolved negative Se isotope excursion in the geologic record, implying at least temporarily suboxic waters in the basin. Furthermore, we find that redox-sensitive element (RSE) enrichments coincide with episodes of P enrichment, thereby implicating a common set of environmental controls on these processes. Together, our dataset implies deposition under a predominantly anoxic water column with periodic fluctuations to more oxidizing conditions because of connections to a large oxic reservoir containing Se oxyanions (and other RSE's, as well as sulfate) in the open ocean. This is broadly consistent with the depositional setting of many modern and recent phosphorites, thereby tying these ancient deposits to a common depositional mechanism. In light of these data, we propose that the broader prevalence of phosphogenesis in the Paleoproterozoic Era was driven by growth of the seawater oxidant reservoir (namely sulfate), thus enabling diagenetic apatite precipitation in basins with high rates of export production, particularly by facilitating the activity of sulfide-oxidizing bacteria. This suggests that the muted authigenic P burial observed in marginal, marine siliciclastic sedimentary rocks during other intervals of the Precambrian was not merely a result of low dissolved P levels in the global deep ocean, but also was influenced by sulfate scarcity and strongly reducing bottom-water conditions.

1. Introduction

Phosphorus (P) is an essential macronutrient and its availability in seawater is thought to exert the dominant control on the rate of marine primary productivity over long (10⁶–10⁹ yr) timescales (Broecker and Peng, 1982; Tyrrell, 1999). Reconstructing marine P levels across Earth's history is thus a major focus of paleo-biogeochemical research, since it may enable an assessment of marine primary productivity in Earth's distant past. To date, several studies have analyzed the P content of ancient marine sedimentary rocks (Bjerrum and Canfield, 2002; Planavsky et al., 2010; Reinhard et al., 2017) and offered quantitative interpretations of the paleo-concentration of P in seawater (Bjerrum and Canfield, 2002; Jones et al., 2015; Konhauser et al., 2007). However, there remains some disagreement as to whether P was scarce or abundant in the Precambrian ocean (Poulton, 2017). Moreover, it is even unclear what mechanism exerted the dominant control on marine

P levels in Earth's early history (Kipp and Stüeken, 2017; Reinhard et al., 2017). The resolution of these issues will thus require an improved understanding of the mechanisms controlling P enrichment in ancient marine sedimentary rocks.

To understand ancient sedimentary P fluctuations and the earliest enrichments observed during the Paleoproterozoic Era (Papineau, 2010), we must first consider the P cycle in the modern ocean. As an essential and rate-limiting nutrient, P is efficiently scavenged in surface waters by phytoplankton (reviewed in Benitez-Nelson, 2000). The dominant supply of P to the ocean is the riverine input of continentally-derived material (Meybeck, 1982), but the recycling of P within the modern ocean proceeds 2–3 orders of magnitude more rapidly than riverine P delivery (Schlesinger and Bernhardt, 2013), thereby extending the marine residence time of P and enabling high rates of primary productivity. The small proportion of P that escapes this recycling process (associated with organic matter exported from the photic zone)

* Corresponding author.

E-mail address: mkipp@caltech.edu (M.A. Kipp).

¹ Present affiliation: The Isotoparium, Division of Geological and Planetary Sciences, California Institute of Technology, Pasadena, CA 91125, USA.

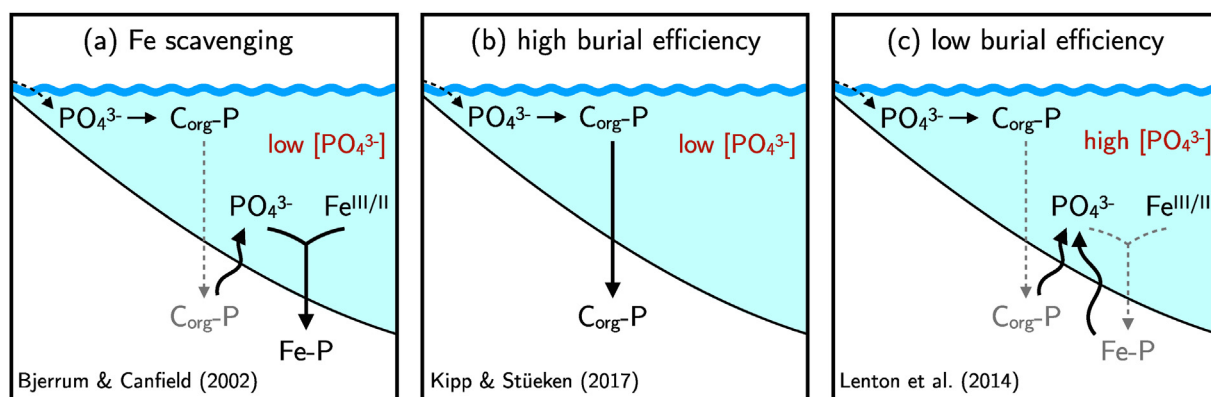


Fig. 1. Proposed mechanisms for limited P burial in Precambrian marine sediments. In (a), P is scavenged from the water column via adsorption to Fe minerals and buried with those phases. In (b), P is buried efficiently with organic carbon due to a scarcity of oxidants for remineralization. In (c), P is not efficiently buried with organic matter or Fe minerals, leading to high marine P levels yet low sedimentary P concentrations. These 3 mechanisms have contrasting implications for C:Fe:P stoichiometry in marine sediments (discussed in Section 1).

is transported to deep waters, and ultimately marine sediments.

Upon reaching marine sediments, P can be buried through multiple pathways (reviewed in Ruttenberg, 2003). First, P can be retained in organic matter if the organic matter escapes remineralization. Second, if organic-bound P is liberated during the oxidation of biomass, P can become sequestered in an inorganic mineral phase. One route for this mineral-trapping of P is the adsorption of P (as orthophosphate, PO_4^{3-}) onto iron (Fe) minerals (Berner, 1973). In the modern, oxygenated ocean, this is typically dominated by Fe-(oxyhydr)oxides (e.g., ferrihydrite; Berner, 1973; Feely et al., 1998). However, reduced or mixed-valence Fe minerals can also bind anions (Zegeye et al., 2012), including phosphate (Hansen and Poulsen, 1999), and so it is thought that these phases could also have scavenged P in the anoxic Precambrian ocean (Derry, 2015; Halevy et al., 2017). Importantly, all these minerals can trap liberated P – either in the water column or sediment porewaters – and immobilize it in sediments. However, if porewater chemistry shifts toward a regime that favors the dissolution of these Fe minerals, P will be released into solution. In addition to the release of the Fe-adsorbed P, porewater P can also be continually supplied through progressive diagenetic remineralization of biomass (Ruttenberg and Berner, 1993). Thus, on diagenetic timescales, P in modern marine sediments typically undergoes a “sink switch,” where liberated P can precipitate as an authigenic apatite mineral phase (predominantly carbonate fluorapatite, CFA) upon accumulating to sufficient porewater concentrations, with a smaller amount of P being incorporated in secondary Fe-(oxyhydr)oxide phases (Poulton and Canfield, 2006; Slomp et al., 1996). So, in sum, P buried in ancient marine sedimentary rocks is predominantly found in the authigenic (apatite) phase, with lesser amounts bound to organic matter or diagenetically-stable Fe minerals (Ruttenberg, 2003).

Despite the many routes for P burial in marine environments, most modern marine sediments have fairly low (< 0.3 wt% P_2O_5) P concentrations (Ruttenberg, 2003) that are similar to the P content of the upper continental crust (0.15 wt% P_2O_5 ; Rudnick and Gao, 2003). This is a testament to the low abundance of P relative to carbon in phytoplankton biomass (i.e., the Redfield ratio, 106 C: 1 P; Redfield, 1958) as well as the selective removal of P from biomass during remineralization (Clark et al., 1998). These processes thus conspire to make P enrichment a rarity in marine sediments. The few modern environments that do promote higher P concentrations (> 1 wt% P_2O_5) tend to favor authigenic precipitation of CFA through a combination of factors (reviewed in Filippelli, 2011; Föllmi, 1996; Ruttenberg, 2003), including (i) high rates of export production (i.e., a large organic-bound P flux to sediments), (ii) high sedimentation rates, which can facilitate burial of organic matter and associated P (Föllmi, 1996; Ingall and Van Cappellen, 1990), (iii) bottom-water redox conditions that are

amenable to CFA precipitation (Jahnke, 1984), and (iv) high phosphate concentrations in porewaters due to the activity of sulfide-oxidizing bacteria (Schulz and Schulz, 2005). In the modern ocean, such conditions tend to be found under regions of nutrient upwelling and high productivity (e.g., the Peru margin, Burnett, 1977; Namibian shelf, Price and Calvert, 1978).

Based on this understanding of P burial in modern marine sediments, an empirical record of P concentrations in ancient marine sediments spanning Earth’s history should be able to inform us about the secular evolution of one or more of the processes controlling P enrichment. Specifically, by tracking the magnitude of P burial through time, we should be able to make inferences about the rate of P export to sediments and prevalence of authigenic P precipitation in ancient marine sediments. Such a record was recently compiled by Reinhard et al. (2017), who showed that the P content of marginal, marine siliciclastic sedimentary rocks was in fact lower in the Precambrian than in the Phanerozoic by a factor of ~4 on average. These authors surmised that the lower P concentrations (and higher C:P ratios) were a result of limited P export to sediments in a low-productivity ocean, which thereby muted the precipitation of authigenic apatite.

While this record clearly demonstrates a shift in the marine P cycle near the end of the Precambrian, some important questions remain. First, the compilation of Reinhard et al. (2017) was filtered to target “typical” marginal marine siliciclastic sedimentary rocks. In doing so, it leaves out most phosphorites, which are extremely P-enriched sedimentary rocks (e.g., Sheldon, 1981). Phosphorites in fact show a significant peak in temporal and spatial abundance during the Paleoproterozoic (Papineau, 2010), suggesting that there was a shift in marine P burial at this time that was distinct from the Archean or mid-Proterozoic.

Second, while the record of P concentrations in marginal marine settings (Reinhard et al., 2017) clearly shows that the rate of P burial was muted in the Precambrian, there are multiple viable interpretations for the dominant mechanism controlling the rate of P burial. Reinhard et al. (2017), following previous workers (Bjerrum and Canfield, 2002; Derry, 2015; Laakso and Schrag, 2014), invoked scavenging of P by Fe-minerals as the main reason for low seawater P levels in the Precambrian (Fig. 1a). As a result, in their modeling scenarios net primary productivity is kept low due to P scarcity (and is accompanied by an imposed increase in the “Redfield” C:P ratio of phytoplankton biomass), thereby limiting export production and the flux of P to sediments (Reinhard et al., 2017). Another mechanism has recently been invoked for Precambrian P scarcity, which postulates that higher burial efficiency in the reducing Precambrian ocean would have limited the recycling of P, thereby promoting efficient P burial with organic matter and low steady-state P concentrations in seawater (Fig. 1b; Kipp and

Stüeken, 2017; Laakso and Schrag, 2018). Lastly, it has also been argued that low P would be expected in Precambrian marine sediments because P burial is ineffective in anoxic settings due to the dissolution of adsorbed P phases and inhibition of CFA precipitation (Ingall and Jahnke, 1994; Poulton, 2017; Van Cappellen and Ingall, 1996). Thus, some authors have cited this mechanism in support of a high-P Precambrian ocean with inefficient burial in sediments (Fig. 1c; Lenton et al., 2014; Poulton, 2017).

Each of these proposed scenarios has slightly different implications for the sedimentary geochemistry of P in the Precambrian (Fig. 1). In the first scenario, P would be expected to co-vary with Fe in many marine sediments. In settings where phosphogenesis was favored (*i.e.*, in certain environments in the Paleoproterozoic), this relationship might break down, with more organic-bound P being sourced to sediments and authigenic phosphate precipitation becoming important. In the second model, P would be expected to occur in stoichiometric proportions with organic matter in most Precambrian marine sediments, with little or no relationship to Fe minerals sourced from the water column. In phosphogenic settings, this relationship would change as authigenic P burial became more important (thus lowering the sedimentary C:P ratio). In the third model, there would not necessarily be a clear preference for P burial with Fe versus organic matter. However, there should be geochemical signatures of high export production in such a high-productivity world, even in non-phosphogenic settings.

Here, we aim to explore these possible controls on P burial in ancient marine sediments. We studied ~2.0 Ga black shales of the Zaonega Formation (ZF) in the Karelia region of NW Russia (Fig. 2). This unit contains abundant organic-rich shales that are thought to have been deposited under predominantly anoxic waters that experienced occasional redox oscillations. Certain horizons of the ZF display large

authigenic P enrichments, in places exceeding 15% P₂O₅ (Lepland et al., 2014), thus representing one of the earliest phosphorites in the geologic record, and perhaps recording more oxidizing conditions. This stratigraphic variability makes the ZF a fitting place to examine the various controls on sedimentary P enrichment in the Precambrian. We present a suite of major and trace element data from the ZF in order to constrain the redox conditions and extent of basinal restriction during deposition. We also present new selenium (Se) abundance and isotopic data to more precisely identify fluctuations across high redox potentials, which could have been important for enabling phosphogenesis. Together, we use this dataset to assess the dominant controls on P burial in Precambrian marine sediments.

2. Materials

2.1. Geologic setting

The Onega Basin of Karelia, NW Russia hosts a large succession of volcanic and sedimentary rocks deposited atop granitic Archean basement in the Paleoproterozoic (Melezhik et al., 2013) (Fig. 2). All units in the Onega Basin were deformed and regionally metamorphosed to greenschist facies during the 1.89–1.79 Ga Svecofennian orogeny (Melezhik and Hanski, 2013); since that time they have been relatively undisturbed on the Russian portion of the Karelian craton. The modern exposure of these units across NW Russia has made them a well-studied archive of Earth system evolution across the interval of rising atmospheric oxygen in the early Paleoproterozoic.

The Zaonega Formation (ZF) lies in the upper portion of the Onega succession (Fig. 3) and is composed of ~1500 m of organic-rich siliciclastic and carbonate sedimentary rocks as well as abundant magmatic

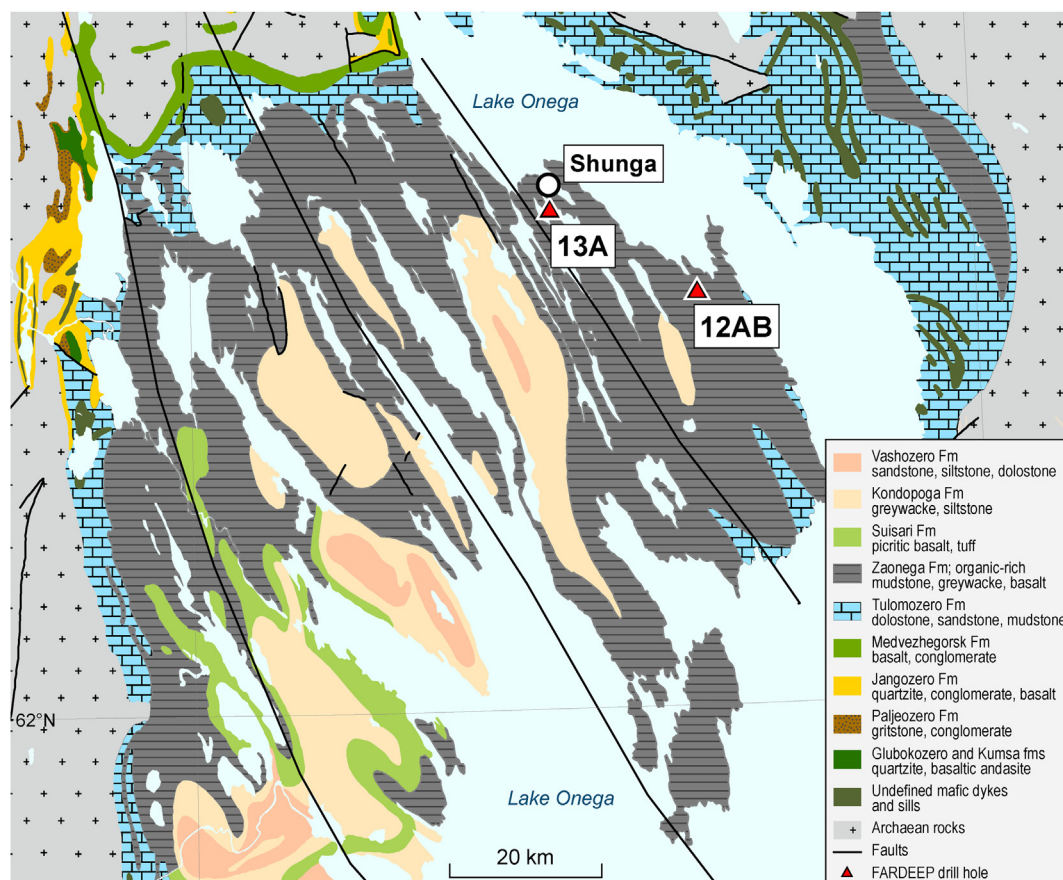


Fig. 2. Geological map of Paleoproterozoic successions in the Onega Basin. Sites of cores 12AB and 13A are marked with red triangles. The Shunga outcrop is near the drilling site of core 13A. Figure modified from Melezhik et al. (2013).

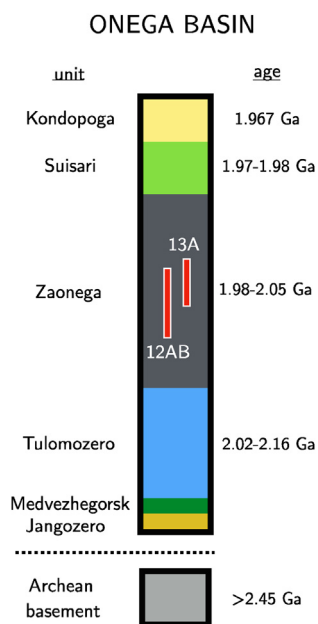


Fig. 3. Stratigraphic context of FAR-DEEP drill cores 12AB and 13A. Ages adapted from Martin et al. (2015) and references therein.

bodies including mafic tuffs, lavas and dolerite sills (Melezhik et al., 2013). The early recognition of high $\delta^{13}\text{C}$ values in carbonates of the Tulomozero Formation, which conformably underlies the ZF, led to an association of these two units with the Lomagundi-Jatuli carbon isotope excursion (Karhu and Holland, 1996; Melezhik et al., 1999a). Specifically, the organic-rich ZF was considered a possible candidate for the elusive sedimentological counterpart to the carbon isotopic evidence for extreme organic carbon burial during the Lomagundi-Jatuli Event (Melezhik et al., 1999b). Since the original identification of these pivotal events, subsequent geochronological work in the Onega Basin has aimed to place them in a firmer temporal context.

The maximum age for all deposition in the Onega Basin comes from a Pb-Pb ID-TIMS date of 2449 ± 1.1 Ma on the Burakovka Pluton (Amelin et al., 1995), which cross-cuts the granitic Archean basement. A lower bound on deposition of the Tulomozero and Zaonega Formations was originally provided by the overlying Suisari magmatic complex, which was dated at 1988 ± 34 via Sm-Nd whole rock + clinopyroxene dating (Puchtel et al., 1998) and 1969 ± 18 Ma via a Re-Os isochron (Puchtel et al., 1999). Carbonates of the Tulomozero Formation were later Pb-Pb dated at 2090 ± 70 Ma (Ovchinnikova et al., 2007), which is consistent with the canonical interpretation of the Lomagundi-Jatuli carbon isotope excursion as a global event lasting from 2220 to 2060 Ma (Karhu and Holland, 1996; Melezhik et al., 1999a). In this view, the organic-rich ZF was thus deposited either during or shortly after the Lomagundi-Jatuli event, consistent with the U-Pb zircon age of 1982 ± 4.5 Ma from a tuff in the lower Zaonega Formation (Martin et al., 2015). This is further corroborated by Pb-Pb dating of zircons from dolerite sills intruding the ZF, which yielded ages of 1919 ± 18 Ma (Priyatkin et al., 2014) and 1956 ± 5 Ma (Stepanova et al., 2014).

For the purpose of this investigation, we adopt a ~ 2.0 Ga age for the ZF, noting that its precise temporal relationship to events in Earth system evolution in the early Paleoproterozoic may be revised by future geochronological work. In any case, though, these rocks clearly post-date the permanent rise of atmospheric oxygen in the Great Oxidation Event (GOE), which occurred at ~ 2.4 Ga (Gumsley et al., 2017); this is supported by an absence of significant mass-independent sulfur isotope fractionation in sedimentary sulfates and sulfides in the Paleoproterozoic succession of the Onega Basin (Blättler et al., 2018; Paiste et al., 2018, 2020; Scott et al., 2014). Furthermore, these sediments were

deposited during an interval of the Paleoproterozoic that was characterized by an increase in phosphorite deposition worldwide (Papineau, 2010).

2.2. Paleo-environmental context

The abundance of magmatic rocks in the ZF indicates deposition in a magmatically-active setting. In addition to interbedded tuffs and late-stage dolerite intrusions, some mafic sills in the ZF display peperite contacts, indicating emplacement into wet and un lithified sediment (Črne et al., 2013b; Galdobina and Sokolov, 1987). Thus, the sedimentary facies of the ZF must be interpreted within the context of this magmatically-influenced dynamic environment.

As noted above, early work inferred that the extremely organic-rich deposits of the ZF (up to tens of percent organic carbon by weight) were indicative of a global organic carbon burial event (Karhu and Holland, 1996; Melezhik et al., 1999a,b). This view was refined by a study of organic carbon and nitrogen isotope ratios in which a step-wise decrease in $\delta^{13}\text{C}_{\text{org}}$ from roughly -25‰ to -40‰ was interpreted as a sign of massive oxidation of sedimentary organic matter resulting from global atmospheric oxygenation (Kump et al., 2011). Since this early work considering the deposition of these organic-rich mudstones in the context of global redox evolution, more detailed regional studies have revealed that local factors likely also contributed to the unique geochemical signals observed in the ZF.

Qu et al. (2012, 2018) analyzed organic carbon isotope ratios throughout the ZF at high stratigraphic resolution and attributed the very negative $\delta^{13}\text{C}_{\text{org}}$ values to methanotrophy occurring via sulfate reduction in a depositional setting experiencing methane seepage. This inference is supported by the abundant evidence of syndepositional magmatism, which readily provides a mechanism for hydrocarbon generation and consumption that is analogous to modern systems (e.g., Niemann et al., 2005; Orphan et al., 2002). One consequence of such vigorous methane cycling could have been depletion of the basinal sulfate reservoir, which is indicated by $\delta^{34}\text{S}$ values in sedimentary sulfides that are typically positive ($+15$ to $+25\text{‰}$; Paiste et al., 2018, 2020; Scott et al., 2014). While depletion of seawater sulfate is difficult to achieve at modern concentrations (~ 28 mM), this could have occurred in the Onega Basin either due to globally low sulfate levels (Scott et al., 2014) and/or because of restricted watermass exchange with the open ocean (thereby cutting off re-supply of sulfate). Transient excursions up to even more positive $\delta^{34}\text{S}$ values (up to $+45\text{‰}$) seem to support the latter scenario (Paiste et al., 2018, 2020), as does the occurrence of massive evaporite deposits in the Onega Basin stratigraphically below the ZF (Blättler et al., 2018).

In the midst of variable basinal restriction and methane seepage, it is conceivable that the redox chemistry of the water column was also characterized by substantial temporal variability. Evidence for such redox fluctuations is indeed found in trace element geochemistry. Kipp et al. (2017) found small Se enrichments and negligible Se isotopic fractionation in organic-rich horizons in the middle part of the ZF, implying local redox conditions that were strongly anoxic and perhaps impacted by basinal restriction. In the same samples, Asael et al. (2013) found muted enrichment and isotopic fractionation of molybdenum (Mo) and uranium (U), consistent with the Se data. However, Lepland et al. (2014) and Mänd et al. (2020) have reported extremely large Mo and U enrichments in the upper part of the ZF. Such stark differences require a substantial change in local and/or global redox chemistry between the deposition of these different portions of the ZF. Joosu et al. (2015) documented negative cerium anomalies in diagenetic apatite from the upper, trace-metal-enriched portion of the ZF, suggesting that this enrichment in trace metals indeed corresponds to evidence for some amount of oxygenated seawater in the basin at that time.

By analogy to modern settings, the evidence for organic matter accumulation and redox fluctuations in the Onega Basin suggest that this setting may have been ripe for phosphogenesis at times. Indeed, the

fact that diagenetic apatite and trace metal enrichments broadly co-occur in the upper ZF (Lepland et al., 2014) seems to support the notion that there is a shared redox-dependence of these processes. However, previous studies have not undertaken a stratigraphically-resolved investigation of various proxies for redox chemistry and basinal restriction. In the present investigation, we aim to use a suite of proxies for paleo-redox conditions and watermass restriction in order to tease apart the various controls on phosphogenesis in the ZF.

2.3. Samples from FAR-DEEP

Samples utilized in this study come from cores that were drilled as part of the Fennoscandia Arctic Russia – Drilling Early Earth Project (FAR-DEEP). In total the FAR-DEEP cores recovered 3600 m of Paleoproterozoic volcanic and sedimentary rocks; two of the cores (12AB, 13A) intersect the middle and upper parts of the ZF (Figs. 2, 3). Both cores 12AB (504 m long) and 13A (240 m long) are predominantly composed of sedimentary rocks, with < 30% of the stratigraphy consisting of magmatic units including tuff beds, dolerite sills, and putative mafic lava flows. The sedimentary rocks of the ZF are commonly very organic-rich, sometimes referred to as “shungite” after the village of Shunga near the site of FAR-DEEP 13A (Melezhik et al., 1999b). This study focuses on the sedimentary rocks from the upper ~300 m of core 12AB and all of core 13A.

The lower portion of core 12AB (> 150 m depth) contains mostly greywackes, marlstones and mudstones, with minor dolostones and mafic intrusions (Črne et al., 2013a). A massive organic-rich rock is present from 136 to 156 m and represents a petrified oil spill. Atop this layer are mudstone-marls and dolerite sills until ~50 m depth. The top ~50 m of the core is composed of organic-rich mudstones and dolostones.

The lowermost portion of core 13A (196–240 m) is composed of mafic sill, followed by ~70 m of moderately organic-rich (0–15% TOC) greywackes, marlstones and mudstones. Mafic sills comprise 86 to 129 m, with thin interbeds of siliciclastic sediments. The upper contact of these intrusive layers (86–91 m) displays a peperite texture indicative of emplacement into unlithified sediment (Črne et al., 2013b). Atop the magmatic rocks is a ~90 m succession of dolostones and organic-rich mudstones.

Additional samples were obtained from a ~7 m outcrop section in an abandoned mining area near Shunga village, close to the drill site of core 13A (Fig. 2). These samples were studied by Lepland et al. (2014) and are extremely enriched in organic matter (up to > 50 wt% TOC) and phosphorus (up to > 15 wt% P₂O₅). Stratigraphically, the outcrop roughly corresponds to the uppermost portion of core 12AB (< 12 m) and the ~35–40 m interval in core 13A (Lepland et al., 2014).

3. Methods

3.1. Major and trace element concentrations

The abundance of major and trace elements was determined by X-ray fluorescence (XRF) spectrometry at the Geological Survey of Norway using the Philips PW 1480 and PANanalytical Axios instruments. For major element analysis, pre-combusted (1000 °C) sample powders were fused to a bead with lithium tetraborate. For trace element analysis, sample powders were mixed with Hoechst wax in a Spex Mixer and then pressed into a pellet. Detection limits were < 0.01% for major element oxides (Al₂O₃, Fe₂O₃, P₂O₅ and TiO₂), < 10 ppm for Mo and U, < 4 ppm for Th, and < 2 ppm for Ni and Cu. The XRF data were also used to constrain Se concentrations prior to isotopic analysis; the detection limit for Se by XRF was < 5 ppm.

Enrichment factors (EF) were calculated for P, Ni, Cu, Mo, U and Se following the approach described by Tribouillard et al. (2006) and Anbar et al. (2007). In all cases, the enrichment factor represents the abundance of the element of interest relative to a detrital tracer in the

sample, normalized to the ratio of that element and its detrital tracer in the upper continental crust, such that

$$X(EF) = \frac{(X_{\text{sample}}/Y_{\text{sample}})}{(X_{\text{crust}}/Y_{\text{crust}})}$$

where X represents the element of interest and Y is its respective detrital tracer.

Following previous work (Anbar et al., 2007; Cole et al., 2017; Tribouillard et al., 2006), aluminum was used as the detrital tracer for Mo, Cu and Se, titanium (TiO₂) was used for P and Ni, and thorium (Th) was used for U. We used the upper crust composition estimate of Rudnick and Gao (2003) in all calculations except for two instances. For the crustal Mo/Al ratio, we followed Anbar et al. (2007) in using the estimate of 0.19 (ppm/wt. %) from Taylor and McLennan (1995) so that our results would be comparable to previously published data. Similarly, for the crustal Se/Al ratio we adopted a value of 0.017 (ppm/wt. %), following recent studies (Koehler et al., 2018; Stüeken et al., 2015a) that used data from Taylor and McLennan (1995) and Li and Schoonmaker (2003), in order for our data to be directly comparable with recent work on Se in Precambrian marine sedimentary rocks.

3.2. Total organic carbon and total sulfur concentrations

Total organic carbon (TOC) and total sulfur (TS) concentrations were measured at the Geological Survey of Norway using a LECO carbon/sulfur analyzer. De-carbonated powders were used for TOC measurements; bulk rock powders were used for TS measurements. The detection limits were < 0.02% for TOC and < 0.01% for TS.

Additional total sulfur measurements on select samples were conducted in IsoLab at the Department of Earth & Space Sciences, University of Washington. Bulk sample powders were weighed into tin cups along with V₂O₅ as a combustion aid. Samples were analyzed on a Eurovector Elemental Analyzer coupled to a ThermoFinnigan MAT253 continuous flow isotope ratio mass spectrometer. The average analytical accuracy of TS measurements, determined by replicate analyses (*n* = 4) of an in-house BaSO₄ standard, was ± 0.2%; average analytical precision was ± 2% (relative error).

3.3. Selenium concentrations and isotope ratios

Bulk rock powders were prepared for measurement of Se stable isotope ratios following published protocols (Stüeken et al., 2013). Rock powders were digested in a combination of HF, HClO₄ and HNO₃. Thiol cotton fiber was used to isolate Se from the digests. Purified Se solutions were treated with aqua regia prior to evaporative concentration for analysis.

Selenium stable isotope ratios were measured using a multiple-collector inductively-coupled plasma mass spectrometer (Nu Instruments) fitted with a hydride generator (Teledyne CETAC Technologies) and housed in the Isotope Geochemistry Laboratory at the Department of Earth & Space Sciences, University of Washington. The operating environment (torch position, carrier gas flow rate, lens voltage potentials) was tuned daily to optimize signal strength and stability. All Se isotope data are reported in delta notation as δ^{82/78}Se values relative to NIST reference SRM 3149 (cf. Carignan and Wen, 2007), because under our analytical protocol masses 82 and 78 are least affected by isobaric interferences (Stüeken et al., 2013).

In-house standard UW-McRae (*n* = 22) and USGS standard SGR-1 (*n* = 10) were analyzed in all analytical sessions. The Se concentrations (3.1 ± 0.4 ppm, 3.3 ± 0.2 ppm) and δ^{82/78}Se values (0.76 ± 0.20‰, -0.13 ± 0.26‰) obtained for these materials are in agreement with previous studies (Kipp et al., 2017; Kurzawa et al., 2017; Mitchell et al., 2012; Stüeken et al., 2013). The average analytical precision (1σ) of all replicate samples was ± 0.24‰ (*n* = 24).

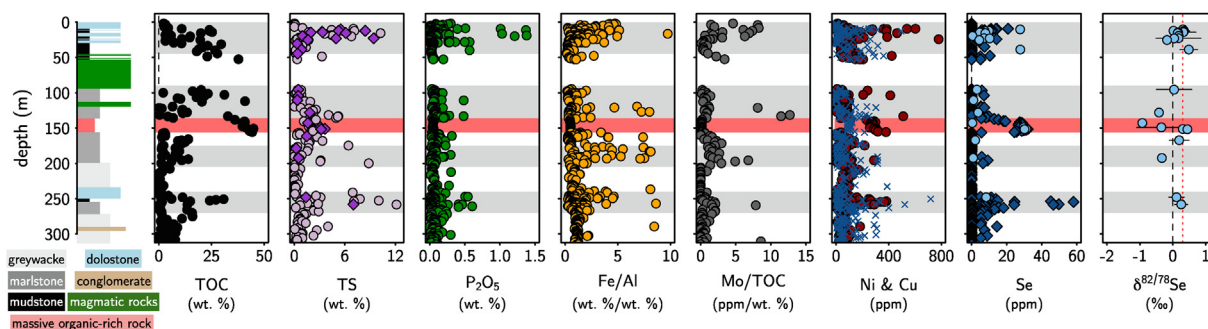


Fig. 4. Chemostratigraphy of FAR-DEEP core 12AB. Grey shaded regions denote intervals of P enrichment. In TS (wt. %) plot, diamonds denote EA data; circles denote LECO data. In Ni & Cu (ppm) plot, red circles denote Ni, blue crosses denote Cu. In Se (ppm) plot, diamonds denote XRF data and circles denote MC-ICP-MS data; dashed line denotes crustal abundance. In $\delta^{82/78}\text{Se}$ plot, dashed line denotes crustal composition, dotted red line denotes modern seawater composition; error bars are 1σ . Detailed description of core 13A can be found in (Črme et al., 2013a).

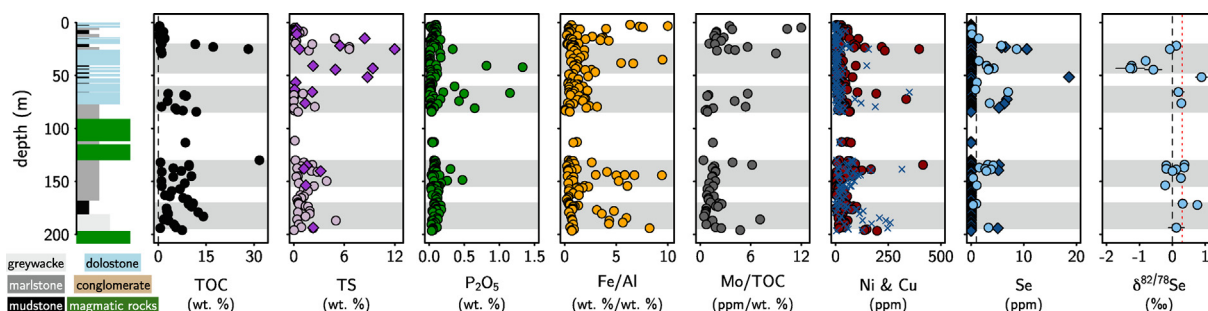


Fig. 5. Chemostratigraphy of FAR-DEEP core 13A. Grey shaded regions denote intervals of P enrichment. Annotations as in Fig. 3. Detailed description of core 13A can be found in (Črme et al., 2013b).

4. Results

The P_2O_5 content of samples from cores 12AB and 13A ranges from 0.01% to 1.38% (Figs. 4, 5). Throughout most of the sedimentary portion of the core, P_2O_5 remains close to average Precambrian shale ($\sim 0.1\%$; Reinhard et al., 2017). Horizons of higher P_2O_5 concentrations are observed in both cores (Figs. 4, 5) as well as in the correlative outcrop section (Fig. 6), where P_2O_5 exceeds 15% (Lepland et al., 2014).

Moderate to weak correlations are observed between P_2O_5 and the detrital tracers TiO_2 (core 12AB: $p < 0.01$, $R^2 = 0.28$; core 13A: $p < 0.01$, $R^2 = 0.10$) and Al_2O_3 (core 12AB: $p < 0.01$, $R^2 = 0.24$; core 13A: $p = 0.05$, $R^2 = 0.03$) in both cores (Fig. 7), though both cores also contain many samples that have distinctly higher $\text{P}_2\text{O}_5/\text{TiO}_2$ and $\text{P}_2\text{O}_5/\text{Al}_2\text{O}_3$ ratios. When normalizing the stratigraphic P trends to TiO_2 , the same horizons of P enrichment are observed (Fig. 8).

The intervals of P enrichment (grey shaded regions in Figs. 4, 5, 8) also feature higher TOC and TS (Figs. 4, 5) as well as greater

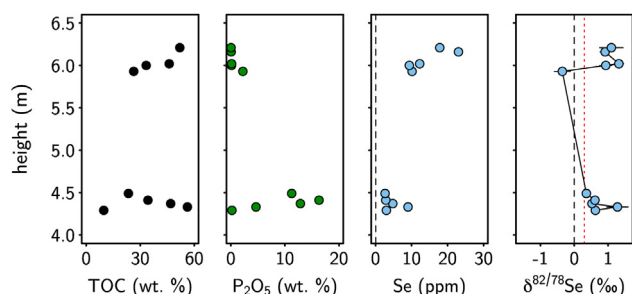


Fig. 6. Chemostratigraphy of outcrop near Shunga village. Outcrop corresponds to $t < 12$ m in core 12AB and 35–45 m depth in core 13A. Annotations as in Figs. 4 and 5. Additional geologic context of outcrop samples can be found in Lepland et al. (2014).

enrichment of Fe, Mo, Ni and Se (Figs. 4, 5) than non-P-enriched intervals. In particular, P enrichments begin around an Fe/Al (wt. %/wt. %) ratio of ~ 0.6 in both cores (Fig. 9) and co-occur with large Mo and U enrichments (Fig. 10).

The abundance of P_2O_5 is weakly correlated with Fe_2O_3 in siliciclastic samples from both cores (core 12AB: $p < 0.01$, $R^2 = 0.19$; core 13A: $p = 0.01$, $R^2 = 0.05$) (Fig. 11A, C). In contrast, P_2O_5 does not strongly correlate with TOC in either core (core 12AB: $p = 0.03$, $R^2 = 0.02$; core 13A: $p = 0.31$) (Fig. 11B, D). The $\text{C}_{\text{org}}:\text{P}$ ratios in both cores are typically greater than 1000, which is much higher than the modern Redfield ratio or the values observed in modern marine sediments (typical $\text{C}_{\text{org}}:\text{P}$ of ~ 250 ; Ruttenberg, 2003).

The abundance of Se in the analyzed samples ranges from 0.1 to 161 ppm (Supplementary Data Files), with larger Se enrichments observed during P-rich intervals than in background intervals (Figs. 4, 5). Throughout both cores, most bulk-rock $\delta^{82/78}\text{Se}$ values are similar to the composition of the continental crust ($\sim 0\%$) and modern seawater ($+0.3\%$) (Figs. 4, 5). Two exceptions are the negative $\delta^{82/78}\text{Se}$ excursions observed at ~ 140 m in core 12AB and at ~ 40 m in core 13A. In core 12AB, the negative excursion reaches a minimum $\delta^{82/78}\text{Se}$ value of -0.93% and occurs across at least 20 m of stratigraphy (148–128 m), mostly occurring within the petrified oil seep interval (Section 2.3; Fig. 4). In core 13A, the negative excursion reaches a minimum $\delta^{82/78}\text{Se}$ value of -1.28% and occurs across at least 9 m of stratigraphy (45–36 m), overlapping with an interval of high P_2O_5 and high P (EF) (Fig. 5). In the outcrop samples, $\delta^{82/78}\text{Se}$ values are similar to or higher than crustal values (Fig. 6).

5. Discussion

5.1. Stratigraphic trends in phosphorus enrichment

The “background” P concentrations throughout much of the ZF are similar to those of roughly co-eval Precambrian marine sediments

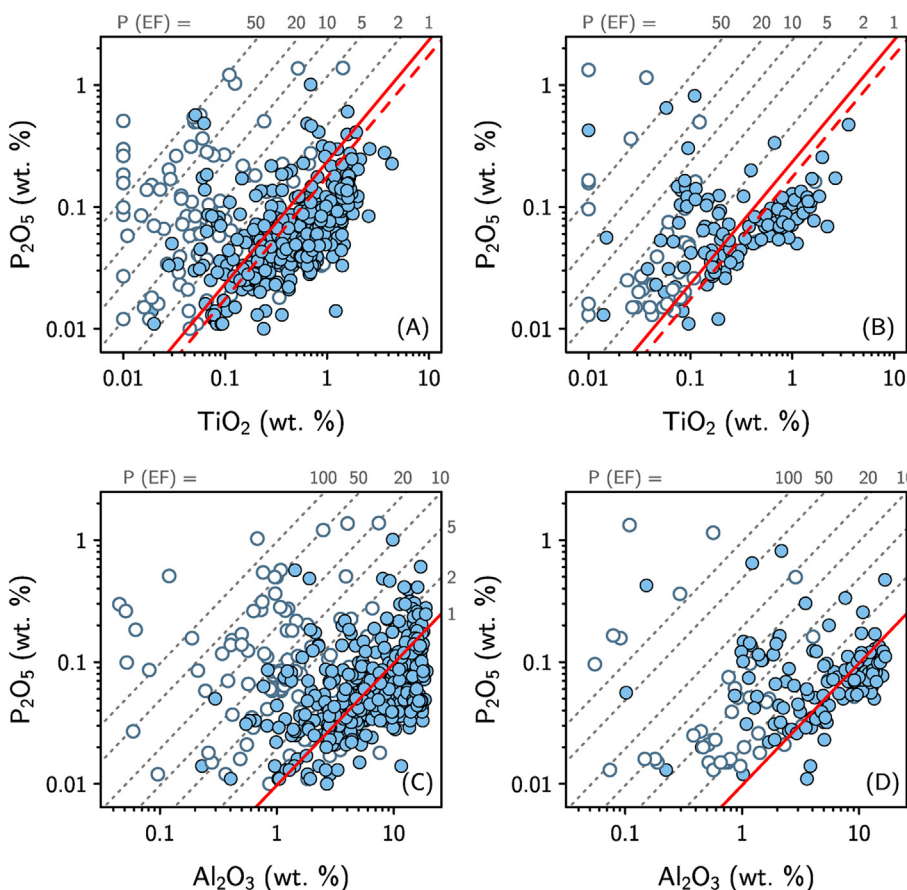


Fig. 7. P₂O₅ versus detrital tracers: TiO₂ in core 12AB (A) and core 13A (B); Al₂O₃ in core 12AB (C) and core 13A (D). White symbols denote carbonates, colored symbols denote siliciclastics. Solid red line denotes P₂O₅/TiO₂ ratio of upper continental crust (Rudnick and Gao, 2003); dashed red line in panels A and B denotes estimated composition of Archean crust (Greber et al., 2017). Grey dotted lines denote contours of P (EF) calculated with each respective detrital tracer, with the most enriched samples plotted toward the top left of the plot.

(Reinhard et al., 2017). For instance, the intervals from 205 to 240 m and > 270 m in core 12AB (Fig. 4), as well as the interval > 150 m in core 13A (Fig. 5) have a mean P₂O₅ concentration of 0.07%, which is similar to the mean of all Precambrian marginal marine siliciclastic sediments observed in Reinhard et al. (2017). Thus, despite the unique geologic setting, background P burial was normal through much of the ZF succession.

However, notable exceptions occur in transient episodes of P-rich sedimentation (grey shaded regions in Figs. 4, 5). In these intervals, P₂O₅ reaches ~0.5% and even exceeds 1% in some cases (Figs. 4, 5). In the outcrop near Shunga village, P₂O₅ reaches > 15% (Fig. 6). In the case of the Shunga outcrop samples, the extremely high P levels and previously-described phosphatic nodules clearly demonstrate that this enrichment is due to diagenetic apatite precipitation (Lepland et al., 2014). For the smaller enrichments observed in the drill cores, we sought to confirm that these are indeed authigenic enrichments (and not artifacts of differential detrital P delivery) by normalizing the P data to titanium (as TiO₂) and aluminum (as Al₂O₃), both of which can be

used as detrital tracers with similar geochemical behavior to P (e.g., Filippelli et al., 2003; Latimer and Filippelli, 2001; Tribouvillard et al., 2006). We note that some studies of P enrichment in recent sediments (e.g., Filippelli et al., 2007) favor normalization to Ti instead of Al, since Al can be preferentially scavenged from the water column during episodes of high biogenic particle flux (Murray et al., 1993; Murray and Leinen, 1996). Thus, we follow these studies in ultimately using Ti normalization to calculate our phosphorus enrichment factors, while acknowledging that each approach has limitations (e.g. Ti can be diagenetically concentrated as authigenic brookite and anatase; Moorad and Aldahan, 1987).

Across all siliciclastic samples (for which normalization to detrital tracers is valid), P₂O₅ is correlated with TiO₂ (Fig. 7A, B) and Al₂O₃ (Fig. 7C, D), perhaps defining trends of varying detrital input. Many samples in fact have lower P₂O₅/TiO₂ ratios than the upper continental crust (< 0.23; Rudnick and Gao, 2003). This likely does not reflect a change in crustal composition, as estimates of Archean crustal P₂O₅/TiO₂ ratios are not substantially different (~0.18; Greber et al., 2017)

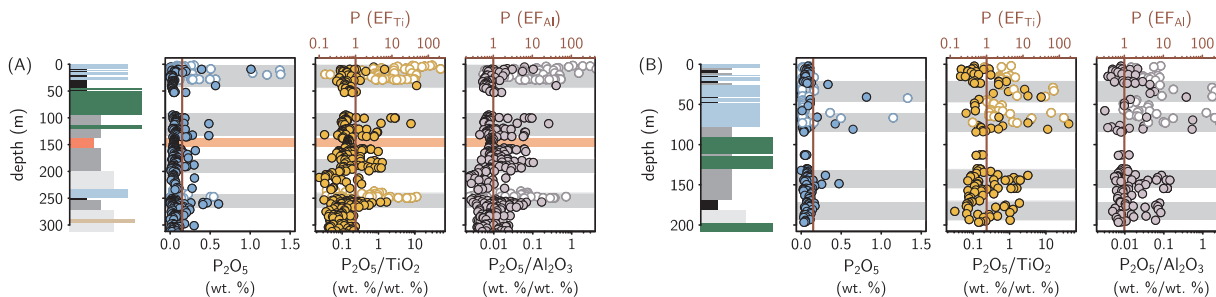


Fig. 8. Profiles of P₂O₅, P₂O₅/TiO₂ and P₂O₅/Al₂O₃ in cores 12AB (A) and 13A (B). White symbols denote carbonates, colored symbols denote siliciclastics. Note log scale in P (EF) plots. Normalizing P₂O₅ to TiO₂ and Al₂O₃ reveals the same intervals of P enrichment.

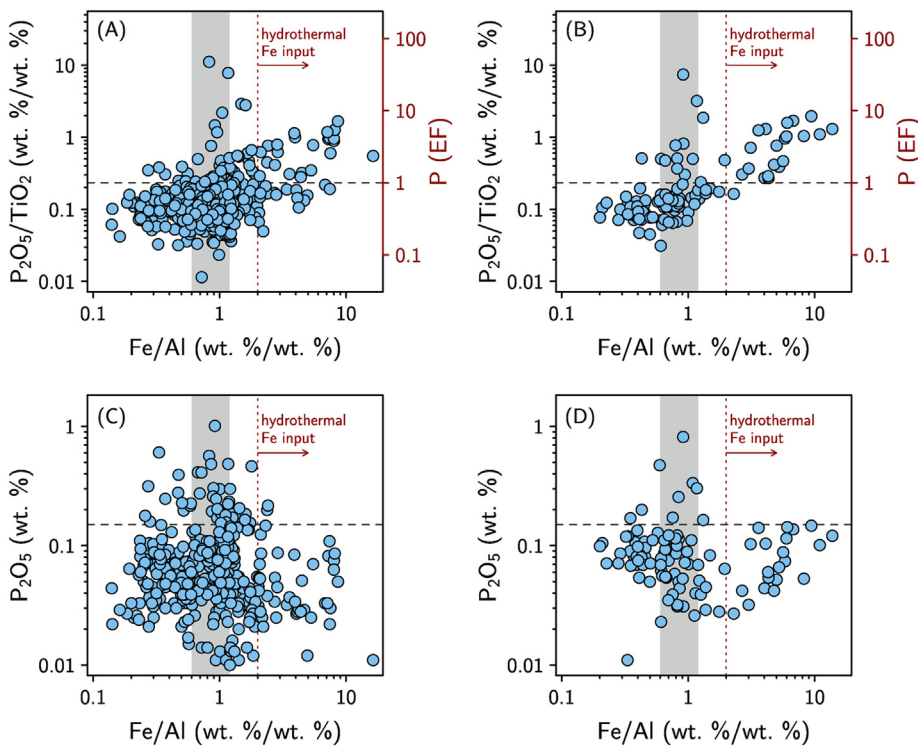


Fig. 9. Phosphorus enrichment (A, B) and P_2O_5 (C, D) vs. Fe/Al in fine-grained siliciclastic samples from core 12AB (A, C) and core 13A (B, D). Grey shaded region denotes range of Fe/Al ratios observed in modern euxinic sediments (Lyons and Severmann, 2006). Dashed horizontal lines denote crustal P_2O_5/TiO_2 ratio (0.234; Rudnick and Gao, 2003), which corresponds to P (EF) = 1 (A, B) and crustal P_2O_5 concentration (0.15 wt%; Rudnick and Gao, 2003) (C, D). Dotted red line and red arrow denote increasing hydrothermal Fe contributions at $Fe/Al \gg 2$ (cf. Raiswell et al., 2018). The largest P enrichments are observed at Fe/Al ratios similar to those of modern euxinic sediments.

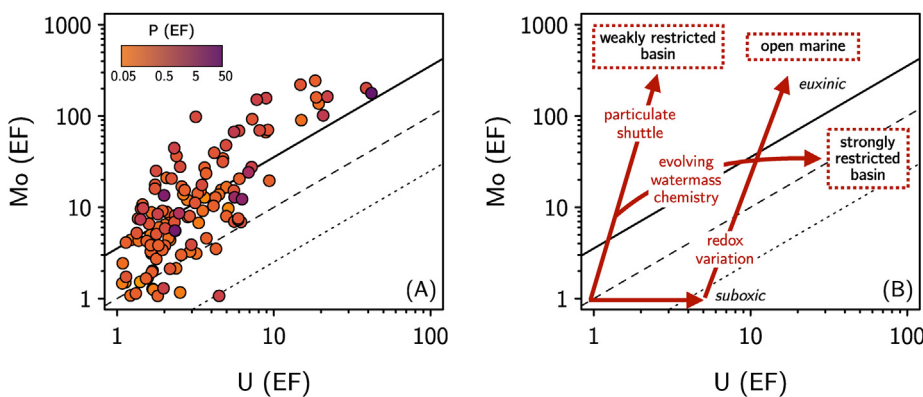


Fig. 10. Mo (EF) vs. U (EF) in fine-grained siliciclastic samples from both cores. Coloration of points denotes P (EF). Panel (B) shows schematic of redox and basinal hydrographic controls on Mo-U co-variation, following Algeo and Tribouillard (2009). Solid line denotes the Mo/U ratio of modern seawater; dashed and dotted lines denote $0.3\times$ and $0.1\times$ the seawater ratio, respectively. The trajectory of samples from both cores follows that expected for a particulate shuttle operating in a weakly restricted basin, with a trend toward stronger restriction and possibly euxinic conditions.

and many samples in our dataset plot below that value as well (Fig. 7A, B). Instead, the very low P levels in these sediments may derive from the fact that P burial is very inefficient in anoxic settings, with P tending to get recycled back into the water column instead of being incorporated in authigenic phases (Ingall and Jahnke, 1994). This is supported by similar trends in P_2O_5 and Al_2O_3 concentrations (Fig. 7C, D). Thus, these data support the notion that limited P burial during the Precambrian was related to inefficient anoxic P burial to some extent (Poulton, 2017).

In contrast, many other samples in our dataset have P_2O_5/TiO_2 and P_2O_5/Al_2O_3 ratios that substantially exceed the crustal value (Fig. 7). These samples are enriched in P relative to the upper continental crust by factors of ~ 10 to > 100 , likely suggesting that ample porewater P availability led to precipitation of diagenetic apatite. This quantification of P enrichment relative to crustal values makes the P_2O_5/TiO_2 ratio useful for considering the environmental controls on P enrichment, which we will explore further below.

Lastly, when the drillcore data are normalized for detrital inputs, the stratigraphic trends resemble those of total P_2O_5 concentrations (*i.e.* enrichments are identified in the same intervals; Fig. 8). The most parsimonious explanation of this similarity is that both parameters are

tracking authigenic P enrichment. The intervals of high P_2O_5 and high P (EF) evidently represent deviations from the “background” conditions, during which times the cycling of P changed such that sedimentary enrichment became feasible. In the rest of the paper, we consider what environmental factors could have enabled certain horizons of the ZF to become enriched in P while others did not.

5.2. Relationship between phosphorus enrichment and redox conditions

One possible explanation for transient episodes of sedimentary P enrichment is that redox conditions shifted to a regime more favorable for phosphogenesis. In modern marine sediments, fluctuating redox conditions can favor phosphogenesis by promoting the activity of sulfide-oxidizing bacteria (*e.g.*, *Thiomargarita* and *Beggiatoa*). These bacteria accumulate phosphate within their cells and occasionally release it to porewaters under more reducing conditions, thereby stimulating diagenetic apatite precipitation (Schulz and Schulz, 2005). These bacteria require porewater sulfide, implicating sulfate reduction within the sediments, as well as a supply of oxidants at the sediment-water interface.

Such a scenario has previously been invoked to explain

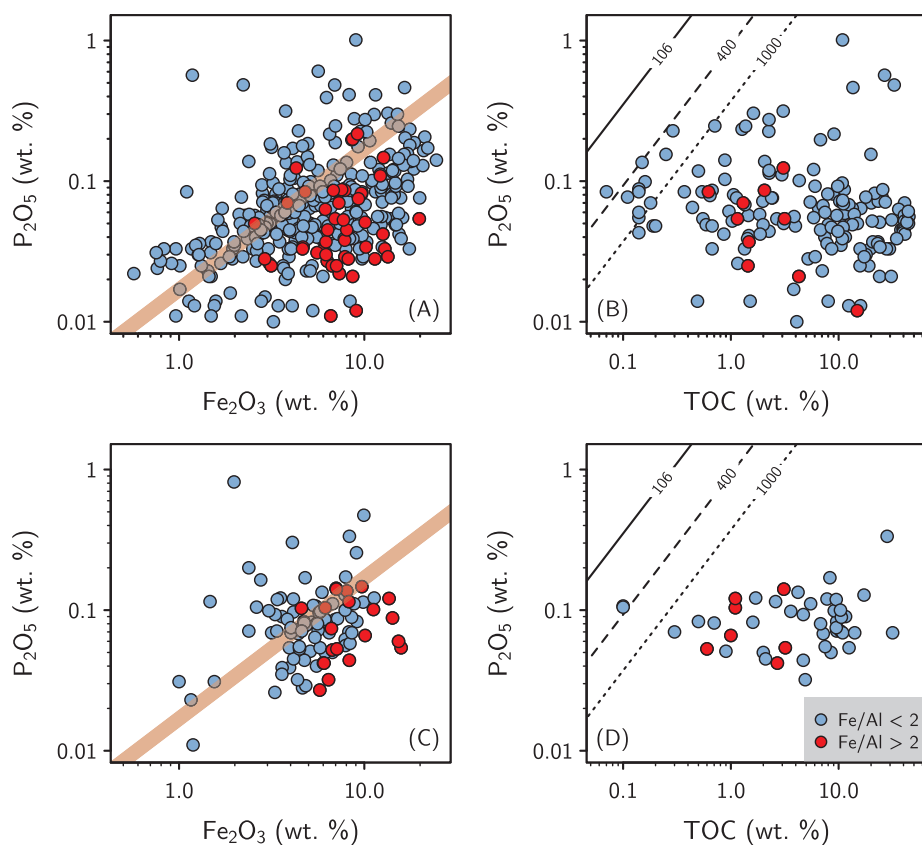


Fig. 11. P_2O_5 vs. Fe_2O_3 (A, C) and P_2O_5 vs. TOC (B, D) in fine-grained siliciclastic samples from core 12AB (A, B) and core 13A (C, D). Red band in panels A and C denotes crustal P_2O_5/Fe_2O_3 ratio (0.167; Rudnick and Gao, 2014). Contours in panels B and D denote molar C:P ratios of 106, 400 and 1000. Red circles denote samples with $Fe/Al > 2$, which is suggestive of hydrothermal Fe input (Raiswell et al., 2018).

phosphogenesis in the ZF on the basis of *Thiomargarita*-sized phosphate nodules as well as large trace metal enrichments suggestive of fluctuating redox conditions (Lepland et al., 2014). In this model, the background conditions in the basin are more strongly anoxic, with periods of redox fluctuations near “suboxic” conditions. Here we explore this hypothesis further using an array of major and trace element proxies with various redox sensitivities.

First we consider the iron to aluminum (Fe/Al) ratio. In the modern ocean, the Fe/Al ratio of siliciclastic sediments increases under reducing conditions, particularly in anoxic and sulfidic (i.e., euxinic) settings, where Fe is efficiently scavenged during pyrite precipitation (Lyons and Severmann, 2006). In modern euxinic settings, such as the Black Sea, Fe/Al ratios range from 0.6 to 1.2 (Lyons and Severmann, 2006). Phanerozoic oxic shales, in contrast, have an average Fe/Al ratio of $\sim 0.53 \pm 0.11$ (Raiswell et al., 2008), which roughly matches the Fe/Al ratio of the upper continental crust (~ 0.5 ; Rudnick and Gao, 2003), reflecting detrital input. Thus, if episodes of P enrichment were associated with the proliferation of sulfur-oxidizing bacteria, which thrive in settings with sedimentary sulfate reduction, we might expect to see P enrichment in intervals with Fe/Al ratios indicative of sulfidic porewaters.

Across the siliciclastic samples in our dataset, P enrichments indeed seem to cluster around the modern euxinic Fe/Al values of 0.6 to 1.2 (Fig. 9A, B). This is consistent with higher sulfate reduction rates during episodes of phosphogenesis in the ZF. The fact that some Fe/Al ratios are much higher than observed in modern euxinic sediments (> 2) may reflect hydrothermal Fe input in these intervals, as this is known to drive $Fe/Al \gg 2$ in modern and recent sediments (Clarkson et al., 2014; Raiswell et al., 2018). In this scenario, sedimentary P enrichment could have been driven by scavenging onto hydrothermal Fe. However, the co-variance of TiO_2 and Al_2O_3 likely explains the positive trend observed at high Fe/Al in Fig. 9A-B; bulk P_2O_5 concentrations in fact peak around the “euxinic” Fe/Al values of 0.6–1.2 (Fig. 9C, D), suggesting that authigenic P burial was more likely facilitated by redox chemistry

in porewaters (i.e. sulfate reduction and sulfide oxidation) than by scavenging of P from the water column by hydrothermally-derived Fe minerals. Thus, we take the Fe/Al data as supportive of the hypothesis that redox fluctuations played a role in mediating phosphogenesis in the ZF.

Another implication of this mechanism – namely, that redox fluctuations supportive of sulfide-oxidizing bacteria were enabling phosphogenesis in the ZF – is that diagenetic sulfide minerals should also be more abundant in the P-rich horizons than in the background intervals. This is precisely the pattern observed in total sulfur concentrations in the drill cores (Figs. 4, 5), and recent work by Paiste et al. (2018, 2020) has demonstrated that the sulfur in correlative horizons of nearby drill cores is predominantly comprised of sedimentary sulfides. Importantly, it is known from sulfur isotope ratios ($\delta^{34}S$) in these sedimentary sulfides of the ZF that the basin was sulfate-limited (Paiste et al., 2018; 2020; Scott et al., 2014). This means that the increases in the rate of sulfate reduction and diagenetic sulfide burial during these episodes were likely driven by growth of the basinal sulfate reservoir, instead of merely a shift in the redox potential of deep waters.

An increase in the size of the basinal sulfate reservoir could have promoted phosphogenesis in multiple ways. First, stimulation of sulfate reduction in sediment porewaters could have promoted the proliferation of sulfide-oxidizing bacteria, which are known to directly mediate phosphogenesis through uptake and release of phosphate (Schulz and Schulz, 2005). Second, sulfate reduction can also indirectly promote diagenetic apatite precipitation by increasing alkalinity in porewaters (Jahnke, 1984). Third, if P burial in the basin was limited due to high burial efficiency during “background” intervals because of a scarcity of oxidants (including sulfate, cf. Kipp and Stüeken, 2017), then an increase in sulfate levels (globally or locally) could have stimulated P recycling and productivity, thereby promoting phosphogenesis.

The latter scenario is consistent with the coincident increases in Ni and Cu in the P-rich horizons (Figs. 4, 5). Both Ni and Cu are predominantly sourced to sediments via organic matter and are efficiently

scavenged under euxinic conditions, meaning that increases in Ni and Cu can reflect higher rates of organic matter export to sediments (Tribouillard et al., 2006). In both cores, enrichments of Ni and Cu are observed in P-rich intervals (Figs. 4, 5). This is consistent with greater organic matter export to sediments during episodes of phosphogenesis; however, other processes are also capable of contributing to Ni and Cu enrichment. Bottom-water euxinia can enhance Ni and Cu scavenging, making it difficult in this case to disentangle the competing role of benthic redox on these enrichments. In both cases, however, the coincident enrichments of Ni and Cu in the P-rich horizons would support the redox mechanism for phosphogenesis in the ZF.

Post-depositional processes can also increase the Ni and Cu content of ancient marine sedimentary rocks. For instance, hypersaline diagenesis of carbonates can cause dolomitization (Machel, 2005) and associated trace metal enrichment via mobilization and re-precipitation (e.g. Kucha and Pawlikowski, 1986). Some of the Ni- and Cu-rich intervals indeed include interbedded dolostones (Figs. 4, 5); however, the most Ni- and Cu-rich samples are in fact those with lower total inorganic carbon (TIC) and higher TS and TOC (Fig. S1). This suggests that precipitation from burial brines is not likely driving the observed stratigraphic trends. Lastly, thermal maturation of ancient marine sediments can cause increases in trace element concentrations due to mass loss of volatile species (e.g. hydrocarbons) (Dickson et al., 2019). However, this is unlikely to explain the stratigraphic trends in Ni and Cu enrichment because there is no evidence for thermal maturity gradients punctuating the same intervals as those of the trace metal enrichments. Thus, while some amount of thermal maturation likely contributed to trace metal enrichments in the ZF, it is unlikely to explain the observed chemostratigraphic trends.

In addition to Ni and Cu enrichments, molybdenum (Mo) is enriched in the P-rich horizons, as shown by large increases in the Mo/TOC ratio (Figs. 4, 5). In the modern ocean, Mo is efficiently scavenged under euxinic conditions (Helz et al., 1996). Across basins with similarly reducing bottom waters, differences in sedimentary Mo/TOC ratios have been shown to correlate with aqueous Mo concentrations (Algeo and Lyons, 2006). The primary driver of these differences is watermass restriction, where more restricted basins tend to progressively deplete their Mo reservoir, leading to a “reservoir effect” where sedimentary enrichments become smaller with time (Algeo and Lyons, 2006). Thus, Mo/TOC can trace either benthic redox and/or the size of the aqueous Mo reservoir.

The higher Mo/TOC ratios in times of P-rich deposition have two possible explanations. First, a shift from anoxic to (at least periodically) euxinic deposition could have promoted more efficient Mo scavenging to sediments. Second, the aqueous Mo reservoir may have grown due to influx of waters from the open ocean. These two scenarios are not mutually exclusive. As mentioned above, the fact that the basin was sulfate-limited implies that episodes of greater sulfate reduction would likely have been stimulated by an influx of sulfate. It is therefore conceivable that a flux of seawater into the basin would have also renewed Mo. Thus, the Mo/TOC trends suggest both seawater Mo and sulfate influx and increasing benthic sulfate reduction rates.

Lastly, we use the Se data to disambiguate between some of the potential interpretations presented above. First, Se is also enriched in the intervals of P enrichment (Figs. 4, 5). As with Mo, this could either result from an increase in scavenging efficiency and/or an increase in the aqueous Se concentration. However, as Se is efficiently scavenged under anoxic (and not just euxinic) conditions (e.g., Cutter, 1982; Rue et al., 1997), and the background deposition of the ZF is thought to have been anoxic (Asael et al., 2013; Scott et al., 2014), it is unlikely that a shift in redox conditions explains the observed Se enrichment trend. Thus, we take the Se enrichments as further support for influx of oxygenated (and oxyanion-enriched) seawater to the basin during episodes of P enrichment.

Second, we note that Se isotopes are not significantly fractionated within most of the P-rich horizons (Figs. 4, 5), with the exception of the

interval near ~40 m in core 13A (which will be discussed below). For the most part, $\delta^{82/78}\text{Se}$ values across both cores fall close to the crustal value (0‰; Stüeken, 2017) and modern seawater composition (+0.3‰; Chang et al., 2017; Stüeken, 2017; Stüeken et al., 2015b). This implies that sequestration of Se in sediments was proceeding efficiently, without a kinetic isotopic preference. Such a scenario is consistent with quantitative oxyanion reduction, which is thought to occur in restricted, anoxic basins in the modern ocean (Stüeken et al., 2015b; Stüeken, 2017) and recent geological past (Kipp et al., 2020). This would further support the inference of basinal restriction, though we note that with a small global Se reservoir in the aftermath of the GOE (Kipp et al., 2017), it is perhaps likely that quantitative Se oxyanion reduction would have been more feasible in open marine settings as well.

There are two notable instances where $\delta^{82/78}\text{Se}$ values do shift markedly. The first is around ~140 m in core 12AB (red shaded region in Fig. 4). This is an anomalous horizon of massive organic-rich rock that has been interpreted as an asphalt effusion onto the seafloor (Qu et al., 2012). The $\delta^{82/78}\text{Se}$ values in this horizon are thus ambiguous, as it is unclear what proportion of the Se was sourced from export production (as typically occurs during marine Se burial) and what proportion derives from the hydrocarbons, which were subject to extensive diagenetic and catagenic re-working that could have altered Se isotope signatures. We therefore do not attempt to interpret this isotopic excursion in the context of water column paleo-redox.

In contrast, another negative $\delta^{82/78}\text{Se}$ excursion occurs near ~40 m in core 13A, coincident with one of the episodes of P enrichment (Fig. 5) and near the stratigraphic height of the extremely P-enriched Shunga outcrop samples. In this case, the sedimentological context (organic-rich dolostone and siltstone) does seem to suggest that the isotopic shift is recording paleo-redox conditions. The fact that $\delta^{82/78}\text{Se}$ is depleted relative to crustal values suggests non-quantitative oxyanion reduction. In the modern ocean, this primarily occurs in open-marine settings where porewater Se reduction is coupled to a large Se supply from oxic ocean water (Mitchell et al., 2012; Stüeken et al., 2015b). Thus, the transition toward lighter Se isotope ratios might reflect a larger aqueous Se reservoir that was not being quantitatively consumed. It could also reflect less-reducing conditions, leading to less efficient Se reduction, which is also consistent with the smaller Se enrichments during the negative isotopic excursion. It is difficult to parse out which of these mechanisms was the dominant control on Se behavior, but it is possible that both were occurring to some extent. Most importantly, though, this negative $\delta^{82/78}\text{Se}$ excursion coincides with P enrichment, suggesting that the redox fluctuations toward suboxic conditions indeed corresponded to times of phosphogenesis.

To summarize, a variety of paleo-redox indicators provide suggestive evidence that conditions shifted from anoxic (but not euxinic) during background intervals to more variable during times of P-enrichment, with higher rates of sulfate reduction and perhaps also periodic supply of oxidants to sediments. These inferences are consistent with previous hypotheses about redox conditions during phosphogenic episodes in the ZF (Joosu et al., 2015; Lepland et al., 2014), but now this array of stratigraphically-constrained geochemical data can be leveraged to address the underlying drivers of redox variability across the ZF. Below we explore one such mechanism.

5.3. Relationship between phosphorus enrichment and basinal restriction

As noted above, the trends in a number of the paleo-redox indicators could potentially be explained by prevailing basinal restriction punctuated by intervals of greater seawater influx to the basin. Higher Fe/Al and TS in P-rich horizons imply that sulfate reduction was promoted in these intervals, likely stimulated by a larger basinal sulfate reservoir. While such transient pulses could be attributed to waxing and waning of the global sulfate reservoir (e.g., Scott et al., 2014), recent work has established that the global marine sulfate reservoir approached about

half its modern size during deposition in the Onega Basin (> 10 mM; Blättler et al., 2018). Such a large reservoir would be well-buffered against rapid, large-magnitude fluctuations in sulfate concentrations, as evidenced by the 10^7 - 10^8 yr periodicity in reconstructions of large-magnitude oscillations in the Phanerozoic sulfate reservoir (Algeo et al., 2015; Berner, 2004; Halevy et al., 2012), consistent with an inferred ~ 20 Myr marine residence time of sulfate (Claypool et al., 1980; Holland, 1973). Thus, we favor an alternative interpretation: that intervals of enhanced communication between the basin and open ocean brought a re-supply of sulfate from the global marine reservoir, thereby stimulating sulfate reduction and the observed transient episodes of redox-sensitive element enrichment and P burial.

Along with sulfate, an influx of seawater would likely have also replenished the supply of macronutrients (i.e., N and P). The existing $\delta^{15}\text{N}$ data from the ZF show only slight changes across the core (Kump et al., 2011), implying consistent aerobic nitrogen cycling in surface waters of the basin – similar to other roughly coeval organic-rich shales that were deposited in open marine settings (Kipp et al., 2018). This suggests that surface waters remained oxygenated and amenable to nitrate accumulation even in the “more restricted” intervals. This is unlike the modern Black Sea, for instance, which has depleted its nitrate reservoir and is dominated by a $\delta^{15}\text{N}$ signature of nitrogen-fixation in its sediments (e.g., Fulton et al., 2012), providing a constraint on the severity of basinal restriction. Although the $\delta^{15}\text{N}$ data do not clearly point to a change in the macronutrient balance of the basin during phosphogenic episodes, the enrichment of Ni and Cu in these intervals suggests that rate of export production was perhaps higher at these times. Thus, it is possible that influx of nutrients stimulated productivity (more likely via P than N) at these times.

Additionally, as noted above, the Mo/TOC and Se data are best explained by growth of the basinal Mo and Se reservoirs during phosphogenic episodes. This is particularly clear for Se, which would have been effectively scavenged during background anoxic deposition, and so likely requires an additional input to explain the large enrichments during phosphogenic episodes. One possible explanation for an increase in aqueous Mo and Se reservoirs is more intense oxidative continental weathering. Such a mechanism could explain the increase in sulfate as well, but this would require large-magnitude global changes in the sulfur cycle, which as mentioned above seems improbable on the timescales under consideration. We thus posit that the trends observed in these major and trace element proxies are better explained by changes in basinal hydrography (specifically, the degree of exchange between the basin and open ocean), where more marine-influenced conditions were co-incident with the episodes of sedimentary P enrichment.

This hypothesis can be further explored using molybdenum-uranium (Mo-U) co-variation, following Algeo and Tribovillard (2009) who pioneered the technique on Paleozoic black shales. The relative enrichment pattern of these elements can be informative of the redox and hydrographic conditions, since each element has distinct processes controlling transport to sediments and also a different abundance in seawater. Specifically, Mo, unlike U, can be transported to sediments via a Mn-oxide “particulate shuttle” when surface waters are oxic (Algeo and Tribovillard, 2009; Crusius et al., 1996; Morford and Emerson, 1999; Murray, 1975). In sediments of weakly restricted basins that deplete some of their trace metal inventory, Mo can thus become more enriched than U due to continued scavenging via Mn-oxides at the chemocline. If such settings become strongly restricted, a trend toward higher U (EF) but constant Mo (EF) is observed, reflecting depletion of the Mo reservoir under restricted conditions and euxinic bottom waters (Fig. 10B). In contrast to restricted basins, open marine settings follow a different trajectory with x-intercepts > 1 U (EF) (Fig. 10B). This is due to the fact that U can be scavenged under suboxic conditions, whereas Mo is only efficiently sequestered in the presence of sulfide (Morford and Emerson, 1999; Tribovillard et al., 2006). As open marine settings transition from suboxic toward anoxic and euxinic conditions, they

follow a trajectory toward equal Mo and U enrichment factors (Fig. 10B). While this technique was developed using sediments deposited after oxygenation of the deep ocean (Algeo and Tribovillard, 2009), and thus has been calibrated to different marine trace metal inventories than are likely to have prevailed in the Paleoproterozoic, the relative pattern of Mo-U enrichment is still likely to hold due to the same removal processes dictating their behavior (i.e., the same redox thresholds).

We find that siliciclastic samples from both cores plot near the “particulate shuttle, weakly restricted basin” trajectory (Fig. 10A). This is consistent with the basin having limited exchange with the open ocean during much of its depositional history. Additionally, the lack of evidence for strong restriction is also consistent with the positive $\delta^{15}\text{N}$ values. There is, however, a slight trend toward the “euxinic” portion of the parameter space (Fig. 10A), suggesting some degree of watermass evolution. This would perhaps be expected during periods of greater communication of the basin with the open ocean and across fluctuating benthic redox conditions. However, within the limited subset of our dataset for which Mo (EF) and U (EF) data are available, there is no clear trend toward higher P (EF) along the trajectory in Mo (EF) vs. U (EF) space (coloration in Fig. 10A). While the inference from the P-rich samples is limited by the sample size, the more general trend reflecting a weakly restricted basin is consistent with the inferred role of basinal hydrography in explaining the geochemical trends observed across the ZF.

To summarize: while no single proxy serves as a definitive indicator of stark changes in basinal circulation between phosphogenic and background conditions, the aggregation of evidence from a diverse array of proxies is better explained by such a mechanism than by invoking global-scale secular changes in oxidant inventories. We thus take this to be the most parsimonious provisional explanation for the control of P enrichment in the ZF.

5.4. Dominant controls on P enrichment: Fe-scavenging, high burial efficiency, or muted anoxic burial?

Finally, we consider whether the observed trends in P enrichment can tell us anything about the dominant mechanism causing limited background P burial in the Precambrian. Precambrian shales average < 0.1 wt% P_2O_5 (Reinhard et al., 2017), in contrast to the P-rich intervals of the ZF where P becomes enriched by up to two orders of magnitude. The fact that redox fluctuations and incursions of open marine waters may have stimulated P enrichment in the ZF can perhaps shed light on what was limiting P burial more broadly in the Precambrian ocean.

At first glance, the role of basinal restriction provides a ready explanation. Since the geologic record is biased toward continental sediments (Husson and Peters, 2018), including restricted epicontinental seaways, it is plausible that the limited P burial observed in the Precambrian is influenced by a lack of data from truly open marine settings. However, this explanation does not explain why P burial increased suddenly in the late Neoproterozoic (Reinhard et al., 2017), or why all sedimentary archives from the Precambrian are generally characterized by low P, even though some are fairly certainly open marine deposits. So this explanation is insufficient, albeit possibly contributing to the observed secular trends.

The traditionally favored mechanism for Precambrian P limitation has been that P was scavenged by Fe minerals in the anoxic Precambrian ocean. Both Fe-oxides (Berner, 1973; Feely et al., 1998) and reduced/mixed-valence Fe minerals (Hansen and Poulsen, 1999; Zegeye et al., 2012) can scavenge dissolved P from seawater, and so could conceivably have restricted the P supply to the biosphere in the photic zone by efficiently transporting Fe-bound P to sediments in the deep ocean. While mid-ocean pelagic settings are not preserved in the earlier Proterozoic rock record, some signature of Fe-scavenging should be retained in marginal marine sediments. We searched for such a

signature by comparing P and Fe concentrations in the siliciclastic samples from the ZF (Fig. 11A, C).

In both cores, weak correlations are observed between P_2O_5 and Fe_2O_3 ($R^2 = 0.19, 0.05$). Most samples have P_2O_5/Fe_2O_3 ratios that are similar to or less than that of the upper continental crust (Fig. 11A, C). Thus, we take these weak correlations as likely signatures of detrital P delivery rather than Fe scavenging from the water column. This is further supported by the fact that samples with Fe/Al ratios > 2 – likely indicative of hydrothermal Fe input (cf. Raiswell et al., 2018) – do not show a significant correlation between P and Fe contents ($p = 0.42, 0.40$). If any samples should show signatures of P scavenging onto Fe minerals, it would likely be those with evidence for elevated Fe input. Thus, in sum, despite observing weak to moderate correlations between P_2O_5 and Fe_2O_3 , we find no obvious evidence for prolonged and substantial scavenging of P from the water column via Fe minerals. In the phosphogenic intervals, in particular, another mechanism must have been transporting P to sediments.

The other viable route of P transport to sediments is via organic matter export. It has been proposed that high burial efficiency of organic carbon (and associated P) could have been the dominant throttle on low Precambrian P levels (Kipp and Stüeken, 2017; Laakso and Schrag, 2018), rather than (or in addition to) Fe-scavenging. In such a model, P might be expected to occur in stoichiometric proportions with organic matter. While the molar C:P ratio of primary producers in the Precambrian is highly uncertain (Planavsky, 2014), we can consider a range of values that spans the modern (C:P = 106) to extremely high (C:P = 1000) to test the plausibility of this mechanism.

In both cores, negligible correlations are observed between P_2O_5 and TOC ($R^2 = 0.02, 0.01$) (Fig. 11B, D). This would seem to suggest that organic matter was not the dominant P source to sediments in background intervals or in times of phosphogenesis. However, there are multiple complicating factors precluding this simple interpretation.

First, the remineralization and maturation of organic matter can variably increase the C:P ratio (Clark et al., 1998; Rutenberg, 2003), thus obscuring the stoichiometric relationship between TOC and P_2O_5 in sediments. Tracers for original organic matter content, such as Ni and Cu, should allow stronger inferences about the relationship between P levels and exported organic matter. As discussed above, the correlation of P enrichment with both Ni and Cu enrichment is suggestive of such a relationship. However, this alone is not conclusive evidence that organic matter dominated the P flux to sediments. In phosphogenic episodes, it is likely that greater organic matter export brought more P to sediments; however, in background intervals, detrital P seems to dominate the signal.

Second, migration of hydrocarbons during and after deposition of the ZF likely played a role in elevating the TOC content of these rocks (Qu et al., 2012, 2018). At the level of individual samples, it is extremely difficult to determine how much of the bulk TOC value comes from indigenous insoluble kerogen and how much from allochthonous migrated bitumen. Thus, it is unclear to what extent the Zaonega $C_{org}:P$ ratios reflect processes akin to those in typical modern marine settings.

While co-variation (or lack thereof) of P_2O_5 with Fe_2O_3 and TOC does not clearly implicate either the Fe-scavenging or limited recycling mechanism for low Precambrian P levels, this dataset can also be used to assess a third model (Fig. 1c): inefficient anoxic P burial (Ingall and Jahnke, 1994) leading to high marine P levels and high Precambrian productivity (Lenton et al., 2014).

The fact that Ni and Cu enrichments are stratigraphically-constrained to the same horizons that feature P enrichment (Figs. 4, 5) suggests an increase in export production at these times. If productivity were in fact high even during background intervals, we might expect to see greater enrichments of Ni and Cu in those intervals than are observed. This doesn't mean that anoxia played no role in setting the efficiency of P burial – the many P_2O_5/TiO_2 ratios plotting below the crustal ratio indicate that background P burial was indeed plagued by recycling of P out of sediments (cf. Ingall and Jahnke, 1994). Rather,

such a mechanism must be co-occurring with one or both of the other mechanisms described above, such that episodes of sedimentary P enrichment are the result of both heightened export production and permissive benthic redox conditions.

5.5. Synthesis: the temporal distribution of phosphorites and secular evolution of the seawater sulfate reservoir

In light of the Zaonega data, we propose an over-arching mechanism for the broader occurrence of phosphorites in the Paleoproterozoic: that growth of the seawater sulfate reservoir caused an expansion of habitats for sulfate-reducing and sulfide-oxidizing bacteria, thereby promoting diagenetic apatite precipitation in sedimentary porewaters on continental shelves or in epicontinental seaways. The fact that our redox proxy data point to higher redox potentials during phosphogenic episodes, with oxidants (namely sulfate) persisting at the sediment-water interface, suggests that there is an important relationship between growth of the oxidant reservoir (i.e., O_2, SO_4^{2-}) in the global ocean and the extent of phosphorite deposition. Furthermore, the evidence for weak basinal restriction in background intervals punctuated by episodic seawater intrusion and introduction of oxidants (including sulfate) during phosphogenic episodes suggests a close temporal relationship between sulfate influx and precipitation of diagenetic apatite. Such a relationship between sulfide-oxidizing bacteria and phosphogenesis has been postulated before for the ZF (Lepland et al., 2014), but now we take this a step further to suggest that the secular record of phosphorite deposition across Earth's history on 10^7 to 10^9 yr timescales could perhaps be related to the waxing and waning of the seawater sulfate reservoir.

Indeed, numerous lines of evidence – including carbonate-associated sulfate (Planavsky et al., 2012), sedimentary sulfide $\delta^{34}S$ values (Scott et al., 2014), and evaporite distributions and geochemistry (Blättler et al., 2018; Schröder et al., 2008) – all point to a growth of the marine sulfate reservoir in the Paleoproterozoic following the GOE. It has long been recognized that a widespread episode of phosphorite deposition occurred at a roughly similar time (e.g., Papineau, 2010); however, a lack of geochronological constraints and stratigraphically-resolved paleo-environmental studies has rendered it difficult to draw a clear causal relationship between growth of the seawater sulfate reservoir and phosphogenesis on a global scale. While the results presented here are only from a single formation, they are best explained by a globally-expanded seawater sulfate reservoir in the Paleoproterozoic that was variably introduced to the Omega Basin during deposition of the ZF (discussed in Section 5.3), thereby implying that similar processes could have been operating to bury P in other basins at this time.

This hypothesis can be tested through future high-resolution paleo-environmental studies of other Paleoproterozoic phosphorites, as well as with targeted work to improve the geochronological constraints on many of these sedimentary successions. Furthermore, this proposal – that growth of the seawater sulfate reservoir enhanced phosphorite deposition – can be further tested by studying the later oxygenation of the oceans during the Neoproterozoic and early Phanerozoic. Many studies of this later interval have invoked an increase in marine sulfate concentrations (e.g., Algeo et al., 2015; Claypool et al., 1980; Halverson and Hurtgen, 2007), and other work has documented extensive phosphorite deposition at the same time (e.g., Cook, 1992; Cui et al., 2016; Donnelly et al., 1990), perhaps suggesting that a similar control on marine P burial may have operated during Earth's second oxygenation event. Unraveling such a first-order control on marine P burial would have important implications for our understanding of the relationship between the oxidation of Earth's surface and the cycling of major nutrients on a planetary scale.

6. Conclusion

We have used major and trace element proxies to show that

sedimentary P enrichment in the ~2.0 Ga Zaonega Formation was influenced by variable redox conditions as well as basinal restriction. The addition of Se abundance data and isotopic ratios to this paleo-redox toolkit enabled disambiguation between possible interpretations, highlighting the utility of this novel proxy. On the one hand, our data suggest that the low P levels observed in Precambrian shales could in some instances be artifacts of deposition in restricted basins. On the other hand, the fact that communication with the open ocean stimulated phosphogenesis in the ZF seems at odds with the generally low P concentrations in other shales of this age. One explanation for this discrepancy is that transient global pulses of oxygenation spurred sporadic phosphogenesis throughout the Paleoproterozoic. Another, perhaps more parsimonious, interpretation is that semi-restricted basins are in some ways favorable for phosphogenesis, which is supported by the occurrence of other phosphorites in epicontinental seaways (Sheldon, 1981). Overall, this work suggests that the record of low P concentrations in marginal marine siliciclastic sedimentary rocks misses some of the dynamic behavior of the P cycle that was occurring during the Precambrian. Importantly, the fact that the first widespread episode of phosphogenesis is restricted to the mid-Paleoproterozoic highlights a significant change in sedimentary P burial at this time. Specifically, this phosphogenic interval indicates that certain basins featured high rates of productivity and persistence of oxidants (namely sulfate) at the sediment-water interface; the disappearance of phosphorites in the later Paleoproterozoic and Mesoproterozoic suggests that such conditions became rare in Earth's middle history. We thus propose that the size of the seawater oxidant reservoir (namely sulfate) exerted a strong first-order control on the extent of phosphorite deposition during the Precambrian. Future high-resolution paleo-environmental studies can help to disentangle the role of marine sulfate fluctuations in mediating phosphogenesis during the Paleoproterozoic as well as in Earth's later history.

Declaration of Competing Interest

The authors declare that they have no known competing financial interests or personal relationships that could have appeared to influence the work reported in this paper.

Acknowledgments

We thank Melanie Mesli and the Norwegian Geological Survey for help with core sampling, as well as Timmu Kreitsmann for help with access to outcrop samples. We also thank Brett Smith, Andy Schauer and Scott Kuehner for technical assistance. MAK acknowledges support from NSF Graduate Research Fellowship DGE-1256082. Funding for this work was provided by NASA Exobiology grant NNX16AI37G to RB.

Appendix A. Supplementary data

Supplementary data to this article can be found online at <https://doi.org/10.1016/j.precamres.2020.105716>.

References

Algeo, T.J., Luo, G.M., Song, H.Y., Lyons, T.W., Canfield, D.E., 2015. Reconstruction of secular variation in seawater sulfate concentrations. *Biogeosciences* 12, 2131–2151.

Algeo, T.J., Lyons, T.W., 2006. Mo–total organic carbon covariation in modern anoxic marine environments: Implications for analysis of paleoredox and paleohydrographic conditions. *Paleoceanography* 21.

Algeo, T.J., Tribouillard, N., 2009. Environmental analysis of paleoceanographic systems based on molybdenum–uranium covariation. *Chem. Geol.* 268, 211–225.

Amelin, Y.V., Heaman, L.M., Semenov, V.S., 1995. U Pb geochronology of layered mafic intrusions in the eastern Baltic Shield: implications for the timing and duration of Paleoproterozoic continental rifting. *Precamb. Res.* 75, 31–46.

Anbar, A.D., Duan, Y., Lyons, T.W., Arnold, G.L., Kendall, B., Creaser, R.A., Kaufman, A.J., Gordon, G.W., Scott, C., Garvin, J., Buick, R., 2007. A whiff of oxygen before the Great Oxidation Event? *Science* 317, 1903–1906. <https://doi.org/10.1126/science.1140325>.

1140325.

Asael, D., Tissot, F.L., Reinhard, C.T., Rouxel, O., Dauphas, N., Lyons, T.W., Ponzevera, E., Liorzou, C., Chéron, S., 2013. Coupled molybdenum, iron and uranium stable isotopes as oceanic paleoredox proxies during the Paleoproterozoic Shunga Event. *Chem. Geol.* 362, 193–210.

Benitez-Nelson, C.R., 2000. The biogeochemical cycling of phosphorus in marine systems. *Earth Sci. Rev.* 51, 109–135.

Berner, R.A., 1973. Phosphate removal from sea water by adsorption on volcanogenic ferric oxides. *Earth Planet. Sci. Lett.* 18, 77–86. [https://doi.org/10.1016/0012-821X\(73\)90037-X](https://doi.org/10.1016/0012-821X(73)90037-X).

Berner, R.A., 2004. A model for calcium, magnesium and sulfate in seawater over Phanerozoic time. *Am. J. Sci.* 304, 438–453.

Bjerrum, C.J., Canfield, D.E., 2002. Ocean productivity before about 1.9 Gyr ago limited by phosphorus adsorption onto iron oxides. *Nature* 417, 159–162.

Blättler, C.L., Claire, M.W., Prave, A.R., Kirsimäe, K., Higgins, J.A., Medvedev, P.V., Romashkin, A.E., Rychanchik, D.V., Zerkle, A.L., Paiste, K., 2018. Two-billion-year-old evaporites capture Earth's great oxidation. *Science* 360, 320–323.

Broecker, W.S., Peng, T.-H., 1982. Tracers in the Sea. Lamont-Doherty Geological Observatory, Columbia University.

Burnett, W.C., 1977. Geochemistry and origin of phosphorite deposits from off Peru and Chile. *Geol. Soc. Am. Bull.* 88, 813–823.

Carignan, J., Wen, H., 2007. Scaling NIST SRM 3149 for Se isotope analysis and isotopic variations of natural samples. *Chem. Geol.* 242, 347–350.

Chang, Y., Zhang, J., Qu, J.-Q., Xue, Y., 2017. Precise selenium isotope measurement in seawater by carbon-containing hydride generation-Desolvation-MC-ICP-MS after thiol resin preconcentration. *Chem. Geol.* 471, 65–73.

Clark, L.L., Ingall, E.D., Benner, R., 1998. Marine phosphorus is selectively remineralized. *Nature* 393, 426–426.

Clarkson, M.O., Poulton, S.W., Guilbaud, R., Wood, R.A., 2014. Assessing the utility of Fe/Al and Fe-speciation to record water column redox conditions in carbonate-rich sediments. *Chem. Geol.* 382, 111–122.

Claypool, G.E., Holser, W.T., Kaplan, I.R., Sakai, H., Zak, I., 1980. The age curves of sulfur and oxygen isotopes in marine sulfate and their mutual interpretation. *Chem. Geol.* 28, 199–260.

Cole, D.B., Zhang, S., Planavsky, N.J., 2017. A new estimate of detrital redox-sensitive metal concentrations and variability in fluxes to marine sediments. *Geochim. Cosmochim. Acta* 215, 337–353.

Cook, P.J., 1992. Phosphogenesis around the Proterozoic-Phanerozoic transition. *J. Geol. Soc.* 149, 615–620.

Črne, A.E., Melezhik, V.A., Prave, A.R., Lepland, A., Romashkin, A.E., Rychanchik, D.V., Hanski, E.J., Luo, Z.-Y., 2013b. Zaonega formation: FAR-DEEP hole 13A. *Front. Earth Sci.* 7, 1008–1046.

Črne, A.E., Melezhik, V.A., Prave, A.R., Lepland, A., Romashkin, A.E., Rychanchik, D.V., Hanski, E.J., Luo, Z.-Y., 2013a. Zaonega formation: FAR-DEEP holes 12A and 12B, and Neighbouring Quarries. *Front. Earth Sci.* 7, 946–1007.

Crusius, J., Calvert, S., Pedersen, T., Sage, D., 1996. Rhenium and molybdenum enrichments in sediments as indicators of oxic, suboxic and sulfidic conditions of deposition. *Earth Planet. Sci. Lett.* 145, 65–78.

Cui, H., Xiao, S., Zhou, C., Peng, Y., Kaufman, A.J., Plummer, R.E., 2016. Phosphogenesis associated with the Shuram Excursion: petrographic and geochemical observations from the Ediacaran Doushantuo Formation of South China. *Sed. Geol.* 341, 134–146.

Cutter, G.A., 1982. Selenium in reducing waters. *Science* 217, 829–831.

Derry, L.A., 2015. Causes and consequences of mid-Proterozoic anoxia. *Geophys. Res. Lett.* 42, 8538–8546.

Dickson, A.J., Idiz, E., Porcelli, D., van den Boorn, S.H.J.M., 2019. The influence of thermal maturity on the stable isotope compositions and concentrations of molybdenum, zinc and cadmium in organic-rich marine mudrocks. *Geochim. Cosmochim. Acta*. <https://doi.org/10.1016/j.gca.2019.11.001>.

Donnelly, T.H., Shergold, J.H., Southgate, P.N., Barnes, C.J., 1990. Events leading to global phosphogenesis around the Proterozoic/Cambrian boundary. *Geol. Soc., London, Spec. Publ.* 52, 273–287.

Feely, R.A., Trefry, J.H., Lebon, G.T., German, C.R., 1998. The relationship between P/Fe and V/Fe ratios in hydrothermal precipitates and dissolved phosphate in seawater. *Geophys. Res. Lett.* 25, 2253–2256. <https://doi.org/10.1029/98GL01546>.

Filippelli, G.M., 2011. Phosphate rock formation and marine phosphorus geochemistry: the deep time perspective. *Chemosphere* 84, 759–766.

Filippelli, G.M., Sierro, F.J., Flores, J.A., Vázquez, A., Utrilla, R., Pérez-Folgado, M., Latimer, J.C., 2003. A sediment–nutrient–oxygen feedback responsible for productivity variations in Late Miocene sapropel sequences of the western Mediterranean. *Palaeogeogr. Palaeoclimatol. Palaeoecol.* 190, 335–348.

Filippelli, G.M., Latimer, J.C., Murray, R.W., Flores, J.-A., 2007. Productivity records from the Southern Ocean and the equatorial Pacific Ocean: testing the glacial shelf nutrient hypothesis. *Deep Sea Res. Part II* 54, 2443–2452.

Föllmi, K.B., 1996. The phosphorus cycle, phosphogenesis and marine phosphate-rich deposits. *Earth Sci. Rev.* 40, 55–124.

Fulton, J.M., Arthur, M.A., Freeman, K.H., 2012. Black Sea nitrogen cycling and the preservation of phytoplankton $\delta^{15}\text{N}$ signals during the Holocene. *Global Biogeochem. Cycles* 26.

Galdobina, L.P., Sokolov, V.A., 1987. The Ludicovian super-horizon. *Geology of Karelia. Nauka (Science), Leningrad* 59–67.

Greber, N.D., Dauphas, N., Bekker, A., Ptáček, M.P., Bindeman, I.N., Hofmann, A., 2017. Titanium isotopic evidence for felsic crust and plate tectonics 3.5 billion years ago. *Science* 357, 1271–1274.

Gumsley, A.P., Chamberlain, K.R., Bleeker, W., Söderlund, U., de Kock, M.O., Larsson, E.R., Bekker, A., 2017. Timing and tempo of the Great Oxidation Event. *PNAS* 114, 1811–1816. <https://doi.org/10.1073/pnas.1608824114>.

- Halevy, I., Peters, S.E., Fischer, W.W., 2012. Sulfate burial constraints on the Phanerozoic sulfur cycle. *Science* 337, 331–334.
- Halevy, I., Alesker, M., Schuster, E.M., Popovitz-Biro, R., Feldman, Y., 2017. A key role for green rust in the Precambrian oceans and the genesis of iron formations. *Nat. Geosci.* 10, 135–139.
- Halverson, G.P., Hurtgen, M.T., 2007. Ediacaran growth of the marine sulfate reservoir. *Earth Planet. Sci. Lett.* 263, 32–44. <https://doi.org/10.1016/j.epsl.2007.08.022>.
- Hansen, H.C.B., Poulsen, I.F., 1999. Interaction of synthetic sulphate “green rust” with phosphate and the crystallization of vivianite. *Clays Clay Miner.* 47, 312–318.
- Helz, G.R., Miller, C.V., Charnock, J.M., Mosselmans, J.F.W., Patrick, R.A.D., Garner, C.D., Vaughan, D.J., 1996. Mechanism of molybdenum removal from the sea and its concentration in black shales: EXAFS evidence. *Geochim. Cosmochim. Acta* 60, 3631–3642.
- Holland, H.D., 1973. Systematics of the isotopic composition of sulfur in the oceans during the Phanerozoic and its implications for atmospheric oxygen. *Geochim. Cosmochim. Acta* 37, 2605–2616.
- Husson, J.M., Peters, S.E., 2018. Nature of the sedimentary rock record and its implications for Earth system evolution. *Emerg. Topics Life Sci.* 2, 125–136.
- Ingall, E., Jahnke, R., 1994. Evidence for enhanced phosphorus regeneration from marine sediments overlain by oxygen depleted waters. *Geochim. Cosmochim. Acta* 58, 2571–2575.
- Ingall, E.D., Van Cappellen, P., 1990. Relation between sedimentation rate and burial of organic phosphorus and organic carbon in marine sediments. *Geochim. Cosmochim. Acta* 54, 373–386.
- Jahnke, R.A., 1984. The synthesis and solubility of carbonate fluorapatite. *Am. J. Sci.* 284, 58–78.
- Jones, C., Nomosatryo, S., Crowe, S.A., Bjerrum, C.J., Canfield, D.E., 2015. Iron oxides, divalent cations, silica, and the early earth phosphorus crisis. *Geology* 43, 135–138.
- Joosu, L., Lepland, A., Kirsimäe, K., Romashkin, A.E., Roberts, N.M., Martin, A.P., Črne, A.E., 2015. The REE-composition and petrography of apatite in 2Ga Zaonega Formation, Russia: the environmental setting for phosphogenesis. *Chem. Geol.* 395, 88–107.
- Karhu, J.A., Holland, H.D., 1996. Carbon isotopes and the rise of atmospheric oxygen. *Geology* 24, 867–870.
- Kipp, M.A., Stüeken, E.E., Bekker, A., Buick, R., 2017. Selenium isotopes record extensive marine suboxia during the Great Oxidation Event. *Proc. Natl. Acad. Sci.* 114, 875–880. <https://doi.org/10.1073/pnas.1615867114>.
- Kipp, M.A., Stüeken, E.E., 2017. Biomass recycling and Earth’s early phosphorus cycle. *Sci. Adv.* 3, eaao4795.
- Kipp, M.A., Stüeken, E.E., Yun, M., Bekker, A., Buick, R., 2018. Pervasive aerobic nitrogen cycling in the surface ocean across the Paleoproterozoic Era. *Earth Planet. Sci. Lett.* 500, 117–126.
- Kipp, M.A., Algeo, T.J., Stüeken, E.E., Buick, R., 2020. Basinal hydrographic and redox controls on selenium enrichment and isotopic fractionation in Paleozoic black shales. *Geochim. Cosmochim. Acta*. <https://doi.org/10.1016/j.gca.2019.12.016>.
- Koehler, M.C., Buick, R., Kipp, M.A., Stüeken, E.E., Zaloumis, J., 2018. Transient surface ocean oxygenation recorded in the ~2.66 Ga Jeerinah Formation, Australia. *Proc. Natl. Acad. Sci.* 115, 7711–7716.
- Konhauser, K.O., Lalonde, S.V., Amiskold, L., Holland, H.D., 2007. Was there really an Archean phosphate crisis? *Science* 315, 1234–1234.
- Kucha, H., Pawlikowski, M., 1986. Two-brine model of the genesis of strata-bound Zechstein deposits (Kupferschiefer type). *Poland. Miner. Deposita* 21, 70–80.
- Kump, L.R., Junium, C., Arthur, M.A., Brasier, A., Fallick, A., Melezhik, V., Lepland, A., Črne, A.E., Luo, G., 2011. Isotopic Evidence for Massive Oxidation of Organic Matter Following the Great Oxidation Event. *Science* 334, 1694–1696. DOI:10.1126/science.1213999.
- Kurzawa, T., König, S., Labidi, J., Yierpan, A., Schoenberg, R., 2017. A method for Se isotope analysis of low ng-level geological samples via double spike and hydride generation MC-ICP-MS. *Chem. Geol.* 466, 219–228.
- Laakso, T.A., Schrag, D.P., 2014. Regulation of atmospheric oxygen during the Proterozoic. *Earth Planet. Sci. Lett.* 388, 81–91.
- Laakso, T.A., Schrag, D.P., 2018. Limitations on limitation. *Global Biogeochem. Cycles* 32, 486–496.
- Latimer, J.C., Filippelli, G.M., 2001. Terrigenous input and paleoproductivity in the Southern Ocean. *Paleoceanography* 16, 627–643.
- Lenton, T.M., Boyle, R.A., Poulton, S.W., Shields-Zhou, G.A., Butterfield, N.J., 2014. Co-evolution of eukaryotes and ocean oxygenation in the Neoproterozoic era. *Nat. Geosci.* 7, 257–265. <https://doi.org/10.1038/ngeo2108>.
- Lepland, A., Joosu, L., Kirsimäe, K., Prave, A.R., Romashkin, A.E., Črne, A.E., Martin, A.P., Fallick, A.E., Somelar, P., Üpraus, K., et al., 2014. Potential influence of sulphur bacteria on Paleoproterozoic phosphogenesis. *Nat. Geosci.* 7, 20.
- Li, Y.H., Schoonmaker, J.E., 2003. Chemical composition and mineralogy of marine sediments. *Treatise Geochem.*
- Lyons, T.W., Severmann, S., 2006. A critical look at iron paleoredox proxies: new insights from modern euxinic marine basins. *Geochim. Cosmochim. Acta* 70, 5698–5722.
- Machel, H.G., 2005. Investigations of burial diagenesis in carbonate hydrocarbon reservoir rocks. *Geosci. Can.* 32, 103–128.
- Mänd, K., Robbins, L.J., Lalonde, S.V., Thoby, M., Paiste, K., Kreitsmann, T., Paiste, P., Reinhard, C.T., Romashkin, A.E., Kirsimäe, K., Lepland, A., Konhauser, K.O., 2020. Paleoproterozoic oxygenated oceans following the Lomagundi-Jatuli Event. *Nat. Geosci.* <https://doi.org/10.1038/s41561-020-0558-5>.
- Melezhik, V.A., Hanski, E.J., 2013. Palaeotectonic and palaeogeographic evolution of Fennoscandia in the Early Paleoproterozoic, in: *Reading the Archive of Earth’s Oxygenation*. Springer, pp. 111–178.
- Melezhik, V.A., Medvedev, P.V., Svetov, S.A., 2013. The Onega Basin, in: *Reading the Archive of Earth’s Oxygenation*. Springer, pp. 387–490.
- Melezhik, V.A., Fallick, A.E., Medvedev, P.V., Makarikhin, V.V., 1999b. Extreme ¹³Ccarb enrichment in ca. 2.0 Ga magnesite–stromatolite–dolomite–red beds’ association in a global context: a case for the world-wide signal enhanced by a local environment. *Earth Sci. Rev.* 48, 71–120.
- Melezhik, V.A., Fallick, A.E., Filippov, M.M., Larsen, O., 1999a. Karelian shungite—an indication of 2.0-Ga-old metamorphosed oil-shale and generation of petroleum: geology, lithology and geochemistry. *Earth Sci. Rev.* 47, 1–40.
- Meybeck, M., 1982. Carbon, nitrogen, and phosphorus transport by world rivers. *Am. J. Sci.* 282, 401–450.
- Mitchell, K., Mason, P.R., Van Cappellen, P., Johnson, T.M., Gill, B.C., Owens, J.D., Diaz, J., Ingall, E.D., Reichart, G.-J., Lyons, T.W., 2012. Selenium as paleo-oceanographic proxy: a first assessment. *Geochim. Cosmochim. Acta* 89, 302–317.
- Moorad, S., Aldahan, A.A., 1987. Diagenetic “replacement” of feldspars by titanium oxides in sandstones. *Sed. Geol.* 51, 147–153.
- Morford, J.L., Emerson, S., 1999. The geochemistry of redox sensitive trace metals in sediments. *Geochim. Cosmochim. Acta* 63, 1735–1750.
- Murray, J.W., 1975. The interaction of metal ions at the manganese dioxide-solution interface. *Geochim. Cosmochim. Acta* 39, 505–519.
- Murray, R.W., Leinen, M., Isern, A., 1993. Biogenic flux of Al to sediment in the central equatorial Pacific Ocean: evidence for increased productivity during glacial periods. *Paleoceanography* 8, 651–670.
- Murray, R.W., Leinen, M., 1996. Scavenged excess aluminum and its relationship to bulk titanium in biogenic sediment from the central equatorial Pacific Ocean. *Geochim. Cosmochim. Acta* 60, 3869–3878.
- Niemann, H., Elvert, M., Hovland, M., Orcutt, B., Judd, A., Suck, I., Gutt, J., Joye, S., Damm, E., Finster, K., 2005. Methane emission and consumption at a North Sea gas seep (Tommeliten area). *Biogeosci. Discuss.* 2, 1197–1241.
- Orphan, V.J., House, C.H., Hinrichs, K.-U., McKeegan, K.D., DeLong, E.F., 2002. Multiple archaeal groups mediate methane oxidation in anoxic cold seep sediments. *Proc. Natl. Acad. Sci.* 99, 7663–7668.
- Ovchinnikova, G.V., Kuznetsov, A.B., Melezhik, V.A., Gorokhov, I.M., Vasil’eva, I.M., Gorokhovskii, B.M., 2007. Pb–Pb age of Jatulian carbonate rocks: the Tulomozero Formation of southeast Karelia. *Stratigraphy and Geological Correlation* 15, 359–372.
- Paiste, K., Lepland, A., Zerkle, A.L., Kirsimäe, K., Izon, G., Patel, N.K., McLean, F., Kreitsmann, T., Mänd, K., Bui, T.H., 2018. Multiple sulphur isotope records tracking basinal and global processes in the 1.98 Ga Zaonega Formation, NW Russia. *Chem. Geol.* 499, 151–164.
- Paiste, K., Pellerin, A., Zerkle, A.L., Kirsimäe, K., Prave, A.R., Romashkin, A.E., Lepland, A., 2020. The pyrite multiple sulfur isotope record of the 1.98 Ga Zaonega Formation: evidence for biogeochemical sulfur cycling in a semi-restricted basin. *Earth Planet. Sci. Lett.* 534, 116092.
- Papineau, D., 2010. Global biogeochemical changes at both ends of the Proterozoic: insights from phosphorites. *Astrobiology* 10, 165–181.
- Planavsky, N.J., 2014. The elements of marine life. *Nat. Geosci.* 7, 855–856.
- Planavsky, N.J., Rouxel, O.J., Bekker, A., Lalonde, S.V., Konhauser, K.O., Reinhard, C.T., Lyons, T.W., 2010. The evolution of the marine phosphate reservoir. *Nature* 467, 1088–1090.
- Planavsky, N.J., Bekker, A., Hofmann, A., Owens, J.D., Lyons, T.W., 2012. Sulfur record of rising and falling marine oxygen and sulfate levels during the Lomagundi event. *PNAS* 109, 18300–18305. <https://doi.org/10.1073/pnas.1120387109>.
- Poulton, S.W., 2017. Biogeochemistry: early phosphorus redigested. *Nat. Geosci.* 10, 75–76.
- Poulton, S.W., Canfield, D.E., 2006. Co-diagenesis of iron and phosphorus in hydrothermal sediments from the southern East Pacific Rise: Implications for the evaluation of paleoseawater phosphate concentrations. *Geochimica et Cosmochimica Acta, A Special Issue Dedicated to Robert A. Berner* 70, 5883–5898. DOI:10.1016/j.gca.2006.01.030.
- Price, N.B., Calvert, S.E., 1978. The geochemistry of phosphorites from the Namibian shelf. *Chem. Geol.* 23, 151–170.
- Priyatkin, N., Khudoley, A.K., Ustinov, V.N., Kullerud, K. are, 2014. 1.92 Ga kimberlitic rocks from Kimozero, NW Russia: Their geochemistry, tectonic setting and unusual field occurrence. *Precamb. Res.* 249, 162–179.
- Puchtel, I.S., Arndt, N.T., Hofmann, A.W., Haase, K.M., Kröner, A., Kulikov, V.S., Kulikova, V.V., Garbe-Schönberg, C.-D., Nemchin, A.A., 1998. Petrology of mafic lavas within the Onega plateau, central Karelia: evidence for 2.0 Ga plume-related continental crustal growth in the Baltic Shield. *Contrib. Miner. Petrol.* 130, 134–153.
- Puchtel, I.S., Brüggemann, G.E., Hofmann, A.W., 1999. Precise Re–Os mineral isochron and Pb–Nd–Os isotope systematics of a mafic-ultramafic sill in the 2.0 Ga Onega plateau (Baltic Shield). *Earth Planet. Sci. Lett.* 170, 447–461.
- Qu, Y., Črne, A.E., Lepland, A., Zuilen, M.A., 2012. Methanotrophy in a paleoproterozoic oil field ecosystem, Zaonega Formation, Karelia, Russia. *Geobiology* 10, 467–478.
- Qu, Y., Lepland, A., van Zuilen, M.A., Whitehouse, M., Črne, A.E., Fallick, A.E., 2018. Sample-scale carbon isotopic variability and diverse biomass in the Paleoproterozoic Zaonega Formation, Russia. *Precamb. Res.* 315, 222–231.
- Raiswell, R., Newton, R., Bottrell, S.H., Coburn, P.M., Briggs, D.E.G., Bond, D.P.G., Poulton, S.W., 2008. Turbidite depositional influences on the diagenesis of Beecher’s Trilobite Bed and the Hunsrück Slate: sites of soft tissue preservation. *Am. J. Sci.* 308, 105–129.
- Raiswell, R., Hardisty, D.S., Lyons, T.W., Canfield, D.E., Owens, J.D., Planavsky, N.J., Poulton, S.W., Reinhard, C.T., 2018. The iron paleoredox proxies: a guide to the pitfalls, problems and proper practice. *Am. J. Sci.* 318, 491–526.
- Redfield, A.C., 1958. The biological control of chemical factors in the environment. *Am. Chem. Geol.* 46, 230A–1221A.
- Reinhard, C.T., Planavsky, N.J., Gill, B.C., Ozaki, K., Robbins, L.J., Lyons, T.W., Fischer, W.W., Wang, C., Cole, D.B., Konhauser, K.O., 2017. Evolution of the global

- phosphorus cycle. *Nature* 541, 386–389. <https://doi.org/10.1038/nature20772>.
- Rudnick, R.L., Gao, S., 2003. Composition of the continental crust. *Treatise Geochem.* 3, 659.
- Rue, E.L., Smith, G.J., Cutter, G.A., Bruland, K.W., 1997. The response of trace element redox couples to suboxic conditions in the water column. *Deep Sea Res. Part I: Oceanogr. Res. Papers* 44, 113–134.
- Ruttenberg, K.C., 2003. The global phosphorus cycle. *Treatise Geochem.* 8, 682.
- Ruttenberg, K.C., Berner, R.A., 1993. Authigenic apatite formation and burial in sediments from non-upwelling, continental margin environments. *Geochim. Cosmochim. Acta* 57, 991–1007.
- Schlesinger, W.H., Bernhardt, E.S., 2013. *Biogeochemistry: An Analysis of Global Change*, third ed. Academic Press.
- Schröder, S., Bekker, A., Beukes, N.J., Strauss, H., Van Niekerk, H.S., 2008. Rise in seawater sulphate concentration associated with the Paleoproterozoic positive carbon isotope excursion: evidence from sulphate evaporites in the 2.2–2.1 Gyr shallow-marine Lucknow Formation, South Africa. *Terra Nova* 20, 108–117.
- Schulz, H.N., Schulz, H.D., 2005. Large sulfur bacteria and the formation of phosphorite. *Science* 307, 416–418.
- Scott, C., Wing, B.A., Bekker, A., Planavsky, N.J., Medvedev, P., Bates, S.M., Yun, M., Lyons, T.W., 2014. Pyrite multiple-sulfur isotope evidence for rapid expansion and contraction of the early Paleoproterozoic seawater sulfate reservoir. *Earth Planet. Sci. Lett.* 389, 95–104. <https://doi.org/10.1016/j.epsl.2013.12.010>.
- Sheldon, R.P., 1981. Ancient marine phosphorites. *Annu. Rev. Earth Planet. Sci.* 9, 251–284.
- Slomp, C.P., Epping, E.H., Helder, W., Raaphorst, W.V., 1996. A key role for iron-bound phosphorus in authigenic apatite formation in North Atlantic continental platform sediments. *J. Mar. Res.* 54, 1179–1205.
- Stepanova, A.V., Samsonov, A.V., Larionov, A.N., 2014. The final episode of the Mid-Paleoproterozoic magmatism in the Omega Basin: data on dolerites in Zaonezhski peninsula. *Pros. Karel. Res. Centre RAS* 1, 3–16.
- Stüeken, E.E., 2017. Selenium isotopes as a biogeochemical proxy in deep time. *Rev. Mineral. Geochem.* 82, 657–682.
- Stüeken, E.E., Foriel, J., Nelson, B.K., Buick, R., Catling, D.C., 2013. Selenium isotope analysis of organic-rich shales: advances in sample preparation and isobaric interference correction. *J. Anal. At. Spectrom.* 28, 1734–1749. <https://doi.org/10.1039/c3ja50186h>.
- Stüeken, E.E., Buick, R., Bekker, A., Catling, D., Foriel, J., Guy, B.M., Kah, L.C., Machel, H.G., Montañez, I.P., Poulton, S.W., 2015b. The evolution of the global selenium cycle: Secular trends in Se isotopes and abundances. *Geochim. Cosmochim. Acta* 162, 109–125. <https://doi.org/10.1016/j.gca.2015.04.033>.
- Stüeken, E.E., Buick, R., Anbar, A.D., 2015a. Selenium isotopes support free O₂ in the latest Archean. *Geology* 43, 259–262. <https://doi.org/10.1130/G36218.1>.
- Taylor, S.R., McLennan, S.M., 1995. The geochemical evolution of the continental crust. *Rev. Geophys.* 33, 241–265.
- Tribouillard, N., Algeo, T.J., Lyons, T., Riboulleau, A., 2006. Trace metals as paleoredox and paleoproductivity proxies: an update. *Chem. Geol.* 232, 12–32.
- Tyrrell, T., 1999. The relative influences of nitrogen and phosphorus on oceanic primary production. *Nature* 400, 525–531.
- Van Cappellen, P., Ingall, E.D., 1996. Redox stabilization of the atmosphere and oceans by phosphorus-limited marine productivity. *Science* 271, 493–496.
- Zegeye, A., Bonneville, S., Benning, L.G., Sturm, A., Fowle, D.A., Jones, C., Canfield, D.E., Ruby, C., MacLean, L.C., Nomosatryo, S., 2012. Green rust formation controls nutrient availability in a ferruginous water column. *Geology* 40, 599–602.